AFCRL 943

Scientific Report 1

PATTERN MEASUREMENTS ON AN EXPERIMENTAL COMPOUND INTERFEROMETER ANTENNA

Prepared for:

ELECTRONICS RESEARCH DIRECTORATE
AIR FORCE CAMBRIDGE RESEARCH LABORATORIES
OFFICE OF AEROSPACE RESEARCH
UNITED STATES AIR FORCE
BEDFORD, MASSACHUSETTS

CONTRACT AF 19(604)-8059

By: W. F. Gabriel

STANFORD RESEARCH INSTITUTE

MENLO PARK, CALIFORNIA

October 1961

AFCRL 943

Scientific Report 1

PATTERN MEASUREMENTS

ON AN EXPERIMENTAL COMPOUND INTERFEROMETER ANTENNA

Prepared for:

ELECTRONICS RESEARCH DIRECTORATE
AIR FORCE CAMBRIDGE RESEARCH LABORATORIES
OFFICE OF AEROSPACE RESEARCH
UNITED STATES AIR FORCE
BEDFORD, MASSACHUSETTS

CONTRACT AF 19(604)-8059

By: W. F. Gabriel

SRI Project No. 3619

Approved:

D. R. SCHEUCH, DIRECTOR ELECTRONICS AND RADIO SCIENCES DIVISION

Copy No.....45

ABSTRACT

An experimental compound interferometer antenna of the "pseudomonopulse" type has been constructed and tested in order to help evaluate its applicability as a possible radar antenna. The antenna consists of eight identical horn-reflector elements that are arranged to provide a compound interferometer aperture measuring 160 wavelengths across. The half-power beamwidth measured about 12 minutes of angle at the operating frequency of 15 gigacycles.

The patterns measured on this experimental model conform quite closely to the patterns predicted by the theoretical analysis, and confirm the basic operating principles of this cross-correlated antenna. The flexibility and ease of receiver control over the effective power pattern proved to be a very interesting feature. Two different sidelobe suppression techniques were tested successfully; one utilizing a nonlinear element at the receiver circuit output, and the other using an automatic channel-signal-balancing servo. It was found that these two techniques were complementary, and that it is advantageous to use them simultaneously. Sidelobe suppression in the range of from 10 db to 40 db was demonstrated.

It is concluded that the natural adaptability of the compound interferometer to sidelobe suppression techniques would permit its use as a radar antenna in those applications where its high resolution and aperture conservation outweigh the disadvantage of a more complicated receiver. The antenna should be particularly attractive at HF and UHF bands, where aperture conservation is of quite some economic importance. Also, it should be useful for communications purposes as well as for radar.

CONTENTS

ABSTRACT ii

LIST OF ILLUSTRATIONS iv

I INTRODUCTION 1

II PATTERN MEASUREMENTS ON AN EXPERIMENTAL COMPOUND INTERFEROMETER ANTENNA 2

A. Description of Antenna 2

B. Alignment of Antenna 6

C. Measurement of sin α/α Linear Power Pattern 11

D. Measurement of Sidelobe Suppression Capabilities Utilizing a Non-Linear Element 20

E. Sidelobe Suppression Obtained Through Use of Automatic Channel Signal Balancing 26

III CONCLUSIONS 36

ACKNOWLEDGMENT 38

REFERENCES 39

ILLUSTRATIONS

Fig. 1	Experimental Compound Interferometer Antenna Mounted on Pattern Range Test Tower	3
Fig. 2	Front Plan-View of Compound Interferometer Antenna . .	4
Fig. 3	Design Sketch of Horn-Reflector Element Used in Compound Interferometer Antenna	4
Fig. 4	E-Plane Pattern of Horn-Reflector 8 (E-Field Perpendicular to Horn Axis)--Frequency 15 Gigacycles .	5
Fig. 5	E-Plane Difference Pattern on Horn-Pair 7 and 8-- Frequency 15 Gigacycles	8
Fig. 6	E-Plane Sum Pattern on Uniformly Illuminated Section Consisting of Horns 1, 2, 3, 4--Frequency 15 Gigacycles	9
Fig. 7	E-Plane Sum Pattern on Interferometer Part Consisting of Horns 5, 6, 7, 8--Frequency 15 Gigacycles	10
Fig. 8	E-Plane Sum Pattern on Complete Compound Interferometer Antenna--Frequency 15 Gigacycles	12
Fig. 9	Block Diagram of Receiver Used for Obtaining Linear Power Patterns on Compound Interferometer	13
Fig. 10	Cathode-Follower Circuit	14
Fig. 11	Subtractor Circuit	15
Fig. 12	E-Plane Linear Power Pattern on Cross-Correlated Compound Interferometer Antenna-- Frequency 15 Gigacycles	18
Fig. 13	Sin α/α Linear Power Pattern Calculated for the Experimental Compound Interferometer Antenna	19
Fig. 14(a)	Sidelobe Suppression Power Patterns on Compound Interferometer Antenna for 0 Volts Bias-- Frequency 15 Gigacycles	22
Fig. 14(b)	Sidelobe Suppression Power Patterns on Compound Interferometer Antenna for 0.2 Volts Bias-- Frequency 15 Gigacycles	23
Fig. 14(c)	Sidelobe Suppression Power Patterns on Compound Interferometer Antenna for 0.4 Volts Bias-- Frequency 15 Gigacycles	24

ILLUSTRATIONS (Concluded)

Fig. 14(d)	Sidelobe Suppression Power Patterns on Compound Interferometer Antenna for 0.6 Volts Bias--Frequency 15 Gigacycles	25
Fig. 15	Block Diagram of Receiver With Simple Electro-mechanical Servo Loop Added to It for Channel Signal Balancing	27
Fig. 16(a)	Sidelobe-Suppression Power Patterns Obtained by Utilizing a Channel Signal Balancing Servo Loop--Servo Off	29
Fig. 16(b)	Sidelobe-Suppression Power Patterns Obtained by Utilizing a Channel Signal Balancing Servo Loop--Servo On	30
Fig. 17(a)	Patterns Taken on Two Simultaneously Transmitting Sources Spaced 13 Feet Apart at a Distance of 1320 Feet. Source A Square-Wave Modulated; Source B Pulse-Modulated and About 17 db Below Source A in Average Power Level. Without Sidelobe Suppression	33
Fig. 17(b)	Patterns Taken on Two Simultaneously Transmitting Sources Spaced 13 Feet Apart at a Distance of 1320 Feet. Source A Square-Wave Modulated; Source B Pulse-Modulated and About 17 db Below Source A in Average Power Level. With Sidelobe Suppression	34

I INTRODUCTION

The compound interferometer is a radio astronomy antenna that has a single-lobed power radiation pattern of the form sin α/α, with approximately half the beamwidth of a conventional antenna of the same aperture dimension. An introductory analysis of this antenna and a discussion of its adaptability to radar use is given in previous reports.[1,2]* There it was found that this antenna could be adapted to radar use by operating it in a "pseudomonopulse" manner. Principal advantages to be gained from using an antenna of this type include high resolution and considerable aperture conservation (reduction in the number of elements), with savings of 75 to 95 percent readily attainable. Principal disadvantages encountered include a high sidelobe level, which forces the implementation of sidelobe suppression techniques, and a somewhat more complex receiver arrangement.

The compound interferometer appeared to offer enough promise as a possible radar antenna to warrant a modest experimental program. Consequently, an experimental antenna was constructed, and its receiver was implemented to the extent permitted by the limited funds available. This simple receiver would not permit a thorough evaluation of the antenna, but at least it did confirm the basic operating principles.

* References are listed at the end of the report.

II PATTERN MEASUREMENTS ON AN EXPERIMENTAL COMPOUND INTERFEROMETER ANTENNA

A. Description of Antenna

The experimental compound interferometer antenna is shown in Fig. 1, mounted on top of its pattern test range tower. A front plan-view of the configuration is shown in Fig. 2. The antenna consists of eight identical horn-reflector elements. Four of these elements are mounted adjacent to one another to form the 40λ uniformly-illuminated section of the aperture (Horns 1, 2, 3, and 4 in Fig. 2), and the remaining four elements are spaced apart by 40λ to form the interferometer section of the aperture (Horns 5, 6, 7, and 8 in Fig. 2). Over-all aperture width is about 160λ, which is large enough to permit close approximation to the aperture illumination functions assumed in the theoretical analysis.[1] To keep the physical dimensions down to a reasonable size, a wavelength of 2 cm (15 Gigacycles) was selected for operating the antenna, so that the over-all antenna width is about ten feet. The eight elements are fed so as to obtain horizontal polarization, and the RG-91/U waveguide feed lines are designed to be of equal length to each element in order to achieve broad bandwidth. All junctions consist of matched hybrid junctions (magic tees) in order to eliminate anti-phase signals and reduce multiple reflections in the plumbing.

The horn-reflector type of element[3] was chosen because of its simplicity of construction, inherent broad bandwidth, ability to utilize any polarization, excellent gain, and good pattern characteristics. Figure 3 is a sketch of the horn-reflector design employed, showing the pertinent dimensions. The horn portion of the element is fabricated from 1/8-inch brass sheet, thus making it rugged enough to retain its accurate pyramidal shape under the usual conditions encountered in handling and testing. The reflector portion of the element consists of a reinforced fibreglass panel which was formed against a very accurate plaster mold. The fibreglass reflector surface is sprayed with silver paint after it is attached to the brass horn.

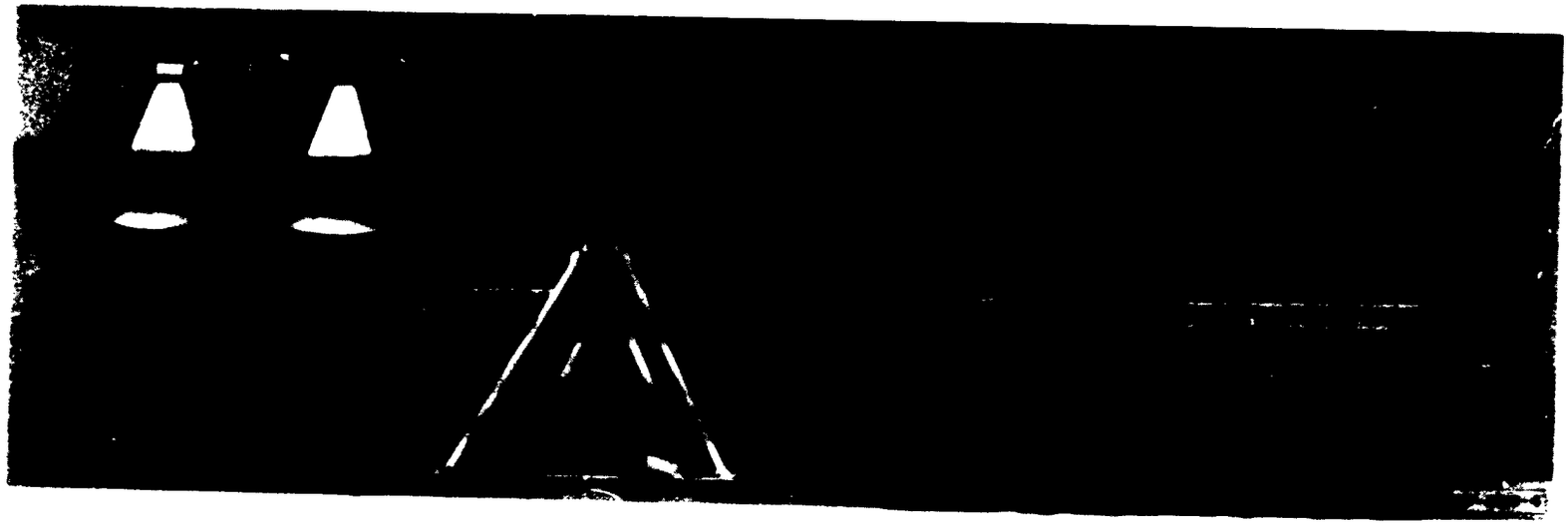

FIG. 1 EXPERIMENTAL COMPOUND INTERFEROMETER ANTENNA MOUNTED ON PATTERN RANGE TEST TOWER

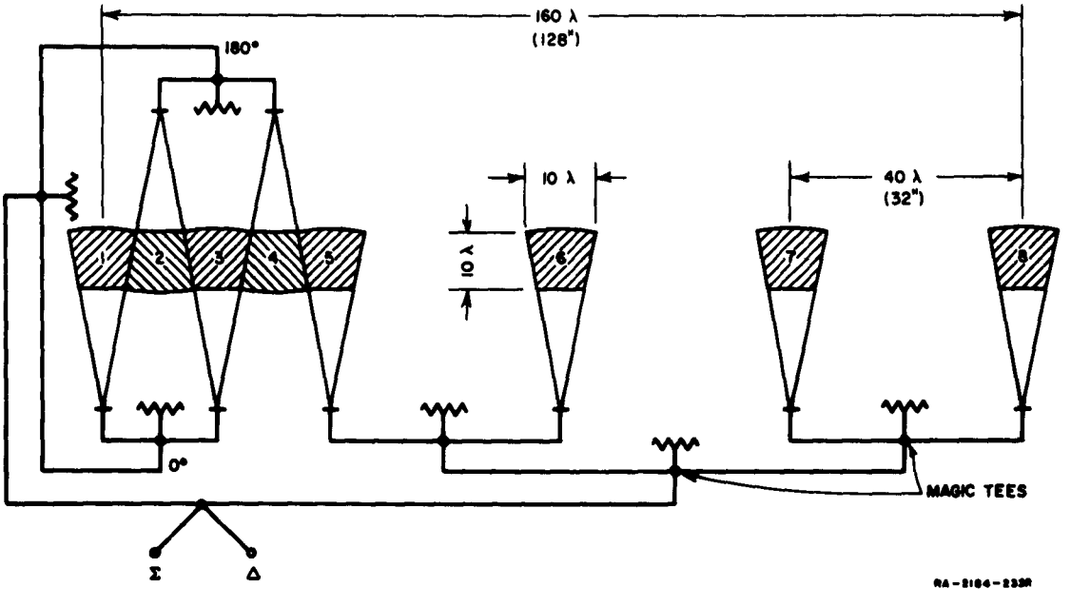

FIG. 2 FRONT PLAN-VIEW OF COMPOUND INTERFEROMETER ANTENNA

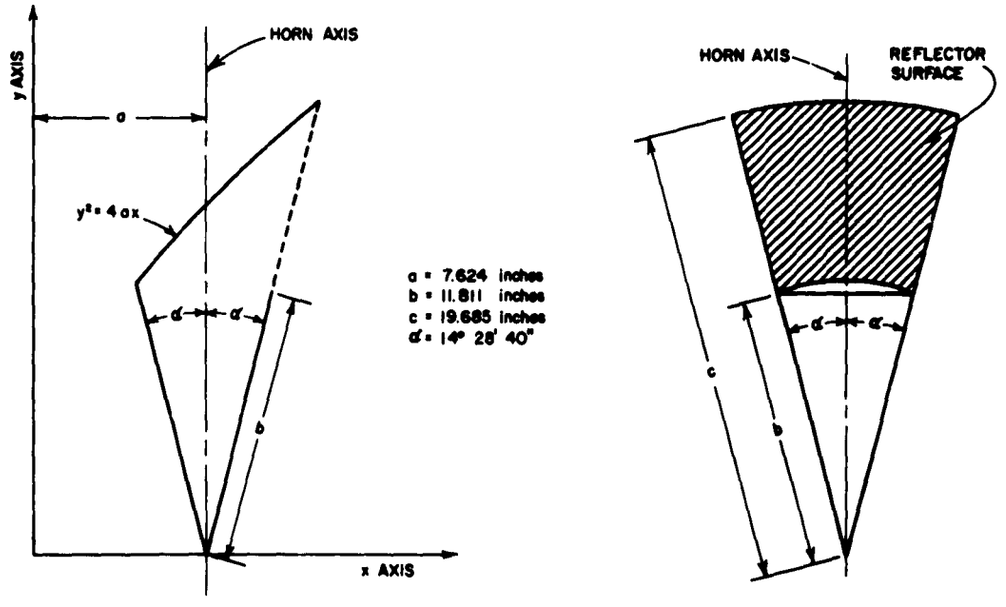

(a) SIDE VIEW IN PLANE OF HORN AXIS, SHOWING SEGMENT OF PARABOLA

(b) FRONT VIEW

FIG. 3 DESIGN SKETCH OF HORN-REFLECTOR ELEMENT USED IN COMPOUND INTERFEROMETER ANTENNA

When operated at 15 Gigacycles, these horn-reflector elements have a gain of about 30 db, and a half-power beamwidth of 5.1 degrees in the E-plane. A typical E-plane pattern is shown in Fig. 4.

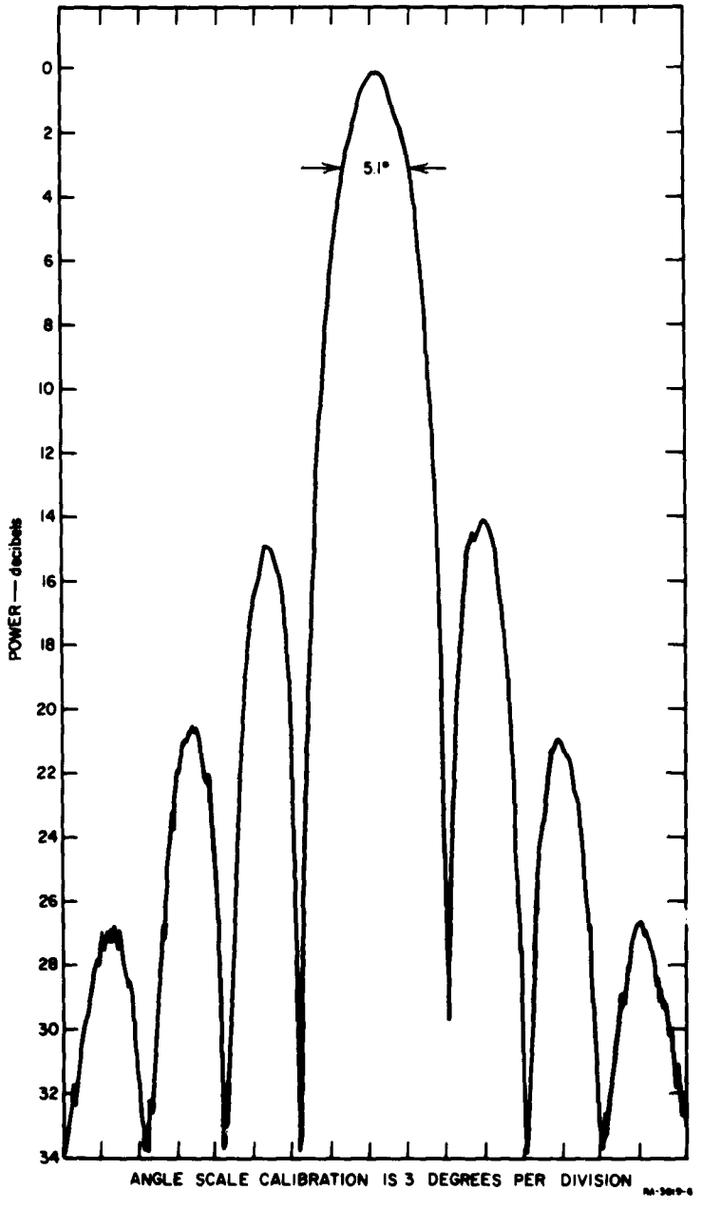

FIG. 4 E-PLANE PATTERN OF HORN-REFLECTOR 8 (E-Field Perpendicular to Horn Axis) – FREQUENCY 15 GIGACYCLES

The eight elements are bolted to a 1/2 x 3-inch steel bar that is, in turn, bolted to a fairly stiff aluminum-channel support structure, thus resulting in a mounting of adequate rigidity.

B. Alignment of Antenna

The alignment of the eight horn-reflector elements was accomplished on the 1320-foot pattern test range at Stanford Research Institute, the longest range available at the time. This distance caused some concern initially because of the fact that it is shorter than the distance normally required to insure safe phase error across the aperture--i.e.,

$$\frac{2D^2}{\lambda} = \frac{2 \times (160\lambda)^2}{\lambda} = 3340 \text{ feet} . \qquad (1)$$

Thus, using the 1320 foot range would require working in the near field of the antenna rather than the far field. However, the criterion represented by Eq. (1) is based upon focussing the antenna at infinity. If the antenna is focussed at a shorter distance instead (in this case, 1320 feet), thus removing the phase error, then the power patterns obtained will very closely approximate the true far-field patterns. Consequently, the horn-reflector elements were positioned by shims so that they were located on a circular arc of 1320 feet radius, rather than being located on a straight line.

Another condition that had to be recognized on this short range was the size of the transmitter antenna. With a final half-power beamwidth of about twelve minutes, the width of the beam at 1320 feet is only five feet. Thus, a transmitter antenna of otherwise reasonable size, such as a three-foot-diameter dish, occupies a large fraction of the beamwidth and can hardly be considered a point source. Looking at this problem in terms of the illumination taper across the ten-foot receiving aperture at 1320 feet, it can be readily calculated that in order to keep the illumination constant within 0.1 db across the receive aperture, the transmitter dish may not exceed eighteen inches diameter. Since the theoretical analysis of the compound interferometer assumes uniform illumination, it was considered necessary to restrict the size of the transmitter antenna to eighteen inches or less in the horizontal plane.

The very narrow beamwidth of the antenna made it necessary to provide an accurate azimuth reference mark to which all patterns could be aligned. This reference was provided in the following manner. A boresight telescope was fixed to the support structure at the center of rotation, or phase center, of the antenna which is located midway between Elements 5 and 6 in Fig. 2 (note that the antenna is asymmetrical). This telescope was accurately shimmed to point in the broadside direction and thus became the optical boresight reference. A microswitch was then arranged with respect to a cam on the mount turntable such that the microswitch would snap on whenever the cross-hairs on the telescope passed through the center of the transmitter antenna as the mount turntable rotated clockwise. The microswitch actuated a marker pen on the pattern recorder, so that a boresight reference mark was present on all patterns and could be utilized to achieve accurate alignment. The marker pen was aligned with the recording pen, of course.

The pattern range equipment used for taking alignment patterns consisted of a square-wave-modulated, 200-milliwatt X-12 klystron transmitting through an eighteen-inch-diameter dish, and on the receive end a 1N78 crystal video detector feeding a tuned 1000-cycle amplifier that drives a 40-db logarithmic, rectilinear recorder.

The first step in the antenna alignment is to get the four pairs of elements (Nos. 1 and 3, 2 and 4, 5 and 6, 7 and 8) accurately pointed at a spot 1320 feet away. This was accomplished by taking difference patterns on each pair, and adjusting the waveguide phase until the central null in the difference pattern was exactly aligned with the reference mark mentioned above. Phase adjustment was obtained by means of a waveguide creasing tool. A typical difference pattern is shown in Fig. 5.

The second step consisted of combining the two pairs of elements (Nos. 1 and 3, 2 and 4) to form the uniformly illuminated section. Here again, difference patterns between the two pairs were taken to obtain accurate alignment of the central null with the reference mark. After final phase adjustment, a sum pattern was taken on this set of four elements, and it is shown in Fig. 6. This sum pattern conforms reasonably

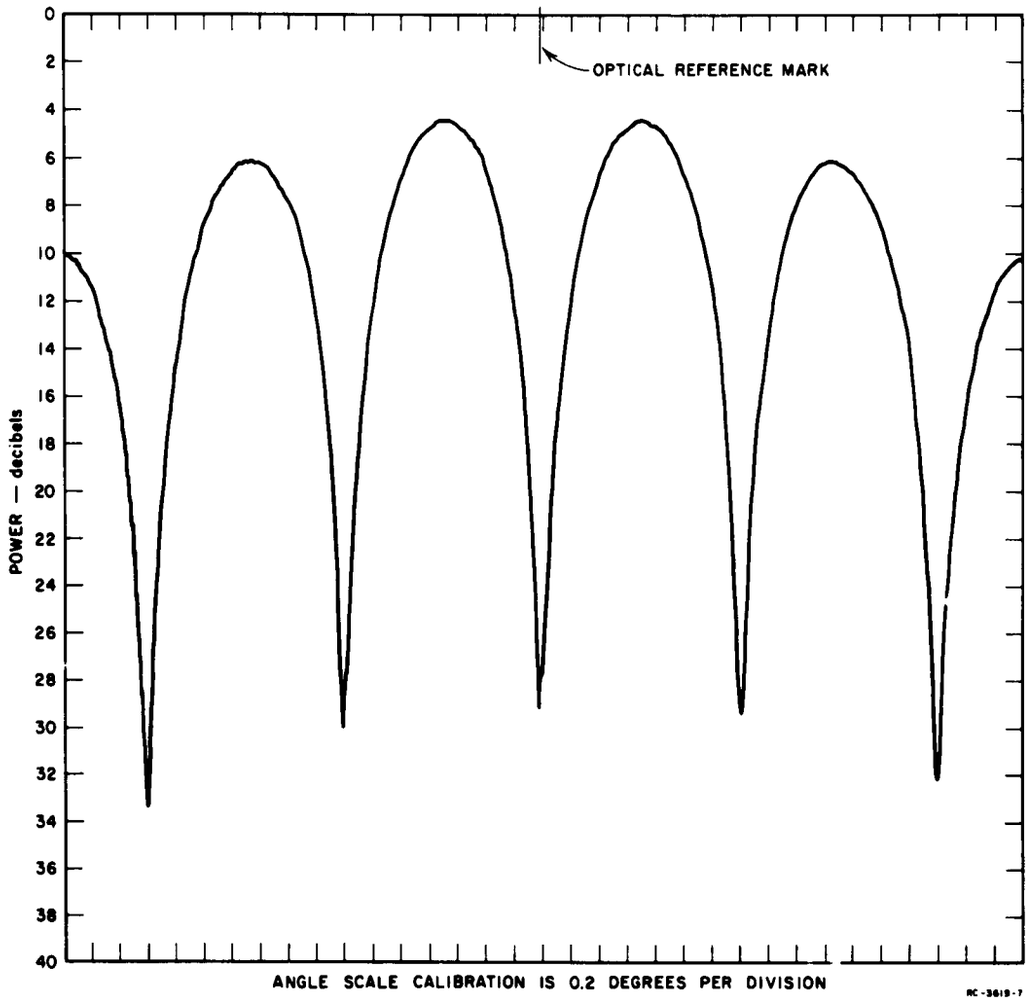

FIG. 5 E-PLANE DIFFERENCE PATTERN ON HORN-PAIRS 7 AND 8 - FREQUENCY 15 GIGACYCLES

well to the theoretical expression assumed for the uniformly illuminated section

$$\left(\frac{\sin u}{u}\right)^2 \qquad (2)$$

where $u = \pi(w/\lambda) \sin \theta$. For this section, $\underline{w}$ has a value of 32 inches.

The third step consisted of combining the two pairs of elements (Nos. 5 and 6, 7 and 8) to form the interferometer portion of the antenna. Difference patterns between the two pairs were taken to obtain accurate

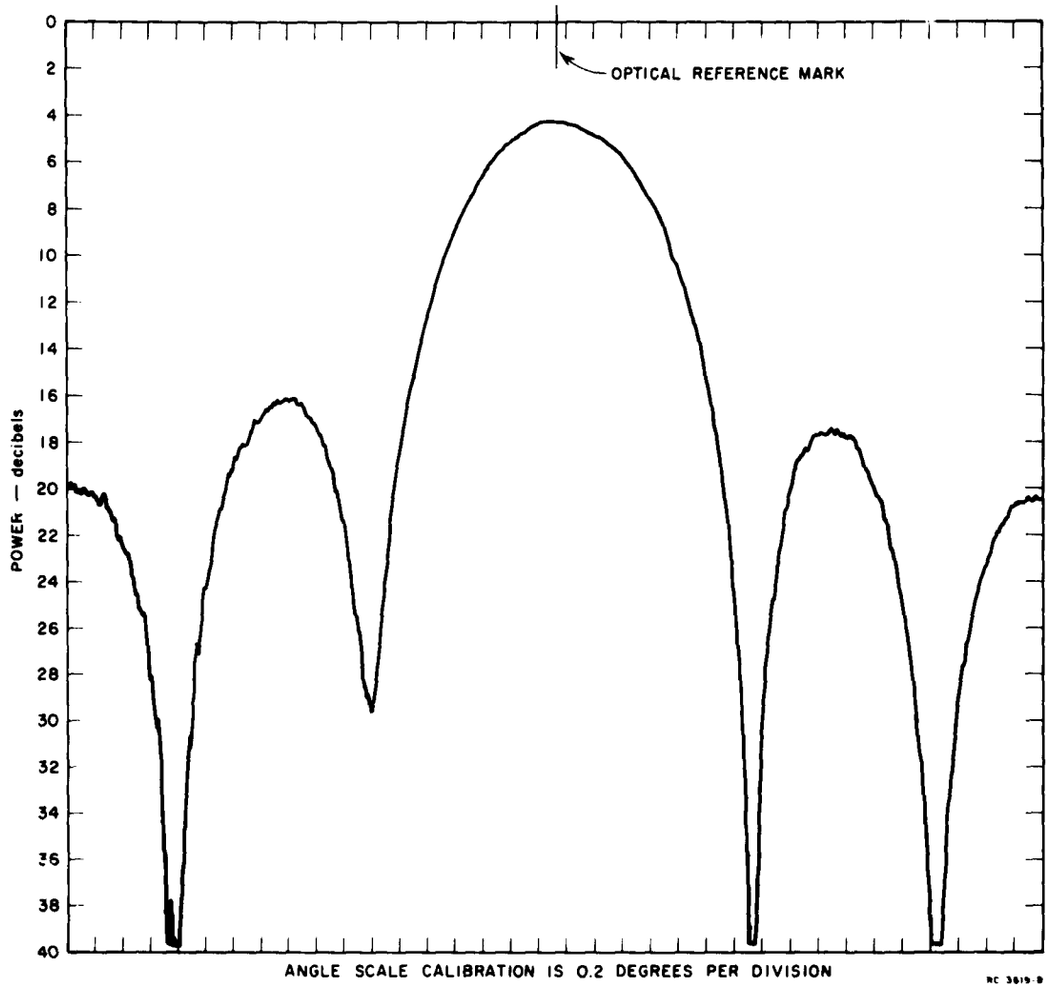

FIG. 6 E-PLANE SUM PATTERN ON UNIFORMLY ILLUMINATED SECTION CONSISTING OF HORNS 1, 2, 3, 4 – FREQUENCY 15 GIGACYCLES

alignment of the central null with the reference mark. After final phase adjustment, a sum pattern was taken on this interferometer and is shown in Fig. 7. This sum pattern conforms reasonably well to the theoretical expression assumed for the interferometer portion

$$\left[\frac{\sin\left(\frac{u}{4}\right)}{\left(\frac{u}{4}\right)} \cdot \cos u \cdot \cos 2u\right]^2 . \qquad (3)$$

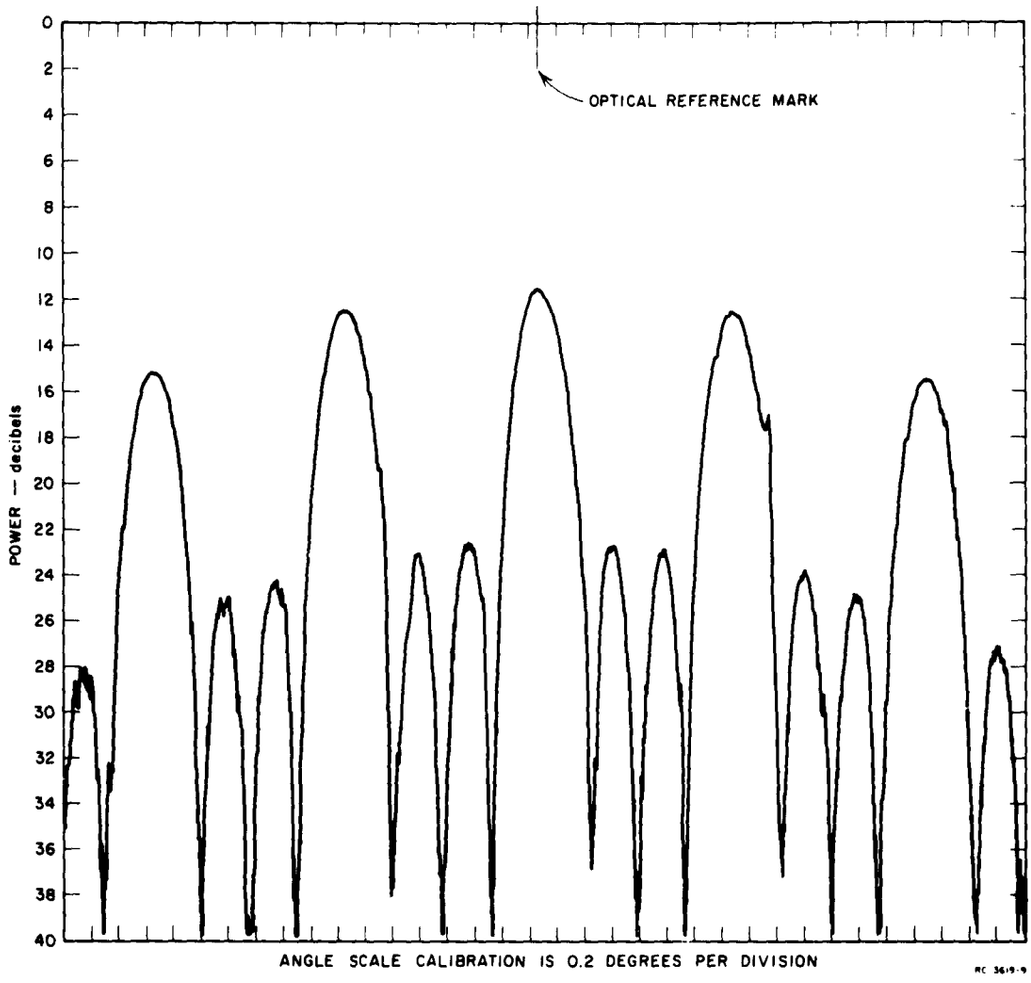

FIG. 7 E-PLANE SUM PATTERN ON INTERFEROMATER PART CONSISTING OF HORNS 5, 6, 7, 8 – FREQUENCY 15 GIGACYCLES

The jerky appearance of portions of this pattern was caused by gusts of wind which created a torque on the antenna and thus perturbed the otherwise constant rate of rotation of the mount turntable.

The fourth step consisted of combining the uniformly illuminated section with the interferometer portion to form the complete compound interferometer antenna as represented in Fig. 2. At this step, one can use either the sum or the difference pattern to achieve final phase adjustment of the connecting waveguide lines, because the symmetry of

the sidelobes is sensitive to phase adjustments. The final sum power pattern, $|\Sigma|^2$, of the compound interferometer antenna is shown in Fig. 8. This sum pattern conforms reasonably well to the theoretical expression[1] calculated for the complete compound interferometer:

$$|\Sigma|^2 = \left\{ \frac{1}{4}\left(\frac{\sin u}{u}\right)^2 + \frac{1}{4}\left[\frac{\sin\left(\frac{u}{4}\right)}{\left(\frac{u}{4}\right)} \cdot \cos u \cdot \cos 2u\right]^2 + \frac{1}{2}\,\frac{\sin\left(\frac{u}{2}\right)}{\left(\frac{u}{2}\right)} \cdot \frac{\sin 8u}{8u}\right\}. \tag{4}$$

Comparison may be made between the logarithmic power pattern in Fig. 8 and the linear power pattern shown in Fig. II-16 of Ref. 1. As a note of interest, the final difference power pattern, $|\Delta|^2$, of the compound interferometer had a boresight direction null that measured -27 db below the peak of the $|\Sigma|^2$ pattern.

The above steps complete the alignment of the antenna, making it ready for use with the receiver circuitry.

C. Measurement of sin α/α Linear Power Pattern

Measurement of the sin α/α linear power pattern requires setting up a receiver that will perform the necessary squaring and subtraction operations, and the arrangement that was decided upon for these measurements is shown in Fig. 9. This simple, video-receiver does not include the IF amplifiers, mixers, and local oscillator that would be included in a fully instrumented, radar-type, pseudomonopulse receiver (see Fig. II-17 of Ref. 1). The reason for omitting these components is that they are not really necessary in demonstrating the principles of operation of the antenna. Thus, the receiver in Fig. 9 starts with the equivalent of the square-law second detector, except that in this case it is detecting the RF energy directly.

The video crystal detectors are preceded by a variable attenuator, the main purpose of which is to adjust the peak RF power level to ten microwatts or less in order to keep the video crystals in their square-law

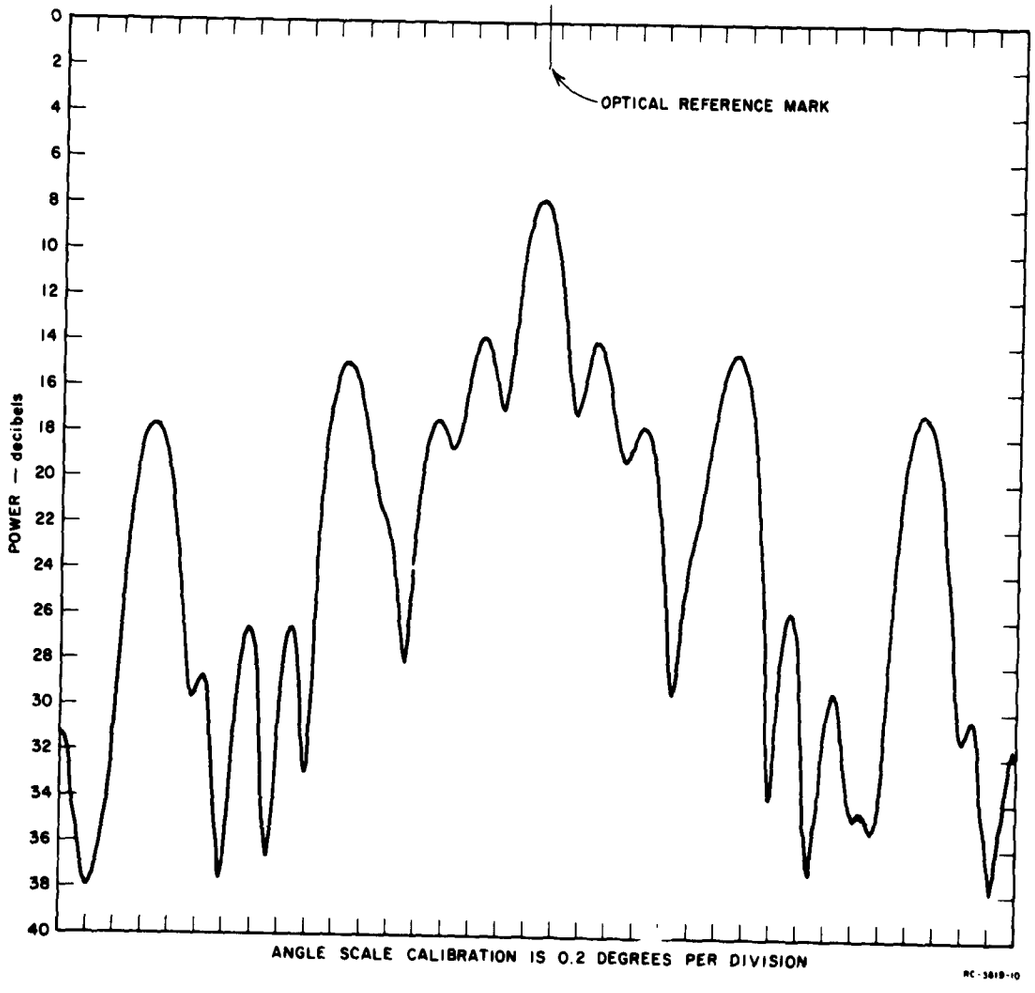

FIG. 8 E-PLANE SUM PATTERN ON COMPLETE COMPOUND INTERFEROMETER ANTENNA – FREQUENCY 15 GIGACYCLES

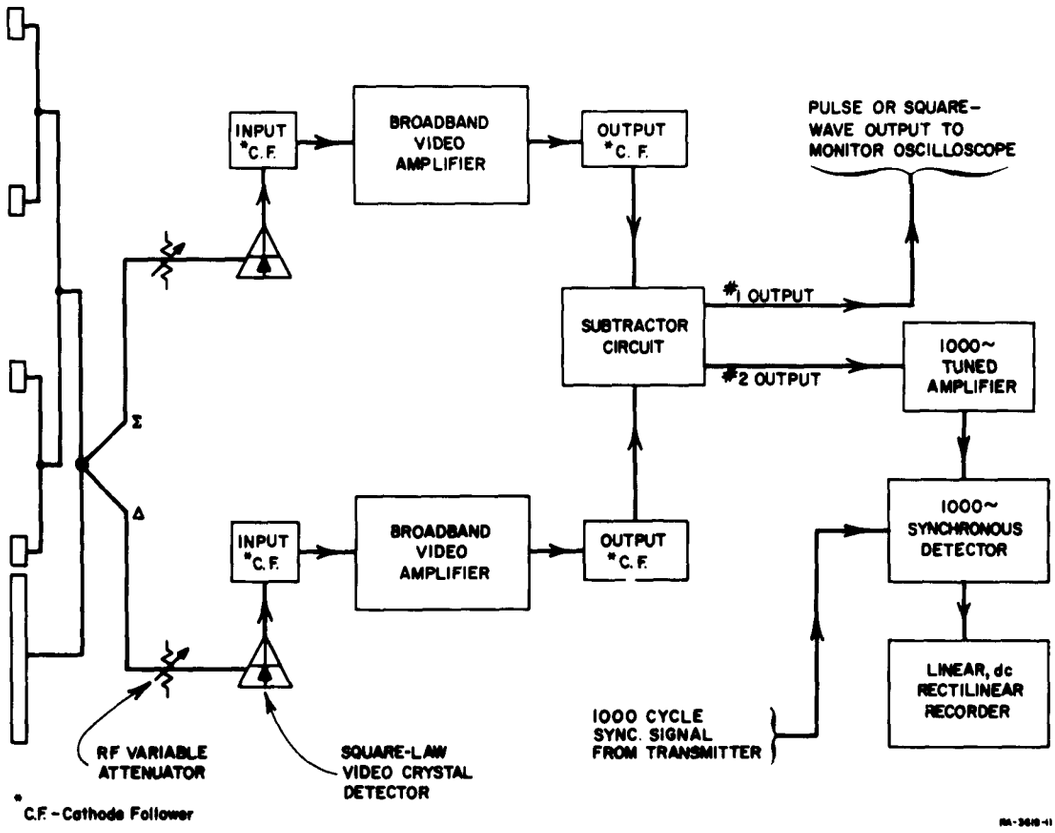

FIG. 9 BLOCK DIAGRAM OF RECEIVER USED FOR OBTAINING LINEAR POWER PATTERNS ON COMPOUND INTERFEROMETER

region. These attenuators also serve as gain controls in the two channels and provide some helpful padding in the sum and difference output arms of the compound interferometer antenna.

In order to transmit detected pulses from the video crystal detectors, which are located on the antenna itself, to the broadband video amplifiers, which are placed on the deck and do not rotate with the antenna, it is necessary to insert an impedance transformer between the video crystal detector and the length of coax line that connects to the broadband video amplifier. The reason for this is that video crystal detectors have a high impedance, typically 5 K to 15 K, so that if one connects a few feet of coax cable (typically 30 μμf per foot) onto them, a low-pass filter is formed and the pulses are stripped of their

high-frequency components. Therefore, an input cathode-follower stage is attached directly to the video crystal detector mount and transforms the impedance down to about 200 ohms with only a small loss in gain. The particular cathode follower design employed is shown in Fig. 10, and is intended to handle ten-microsecond pulses and also square waves.

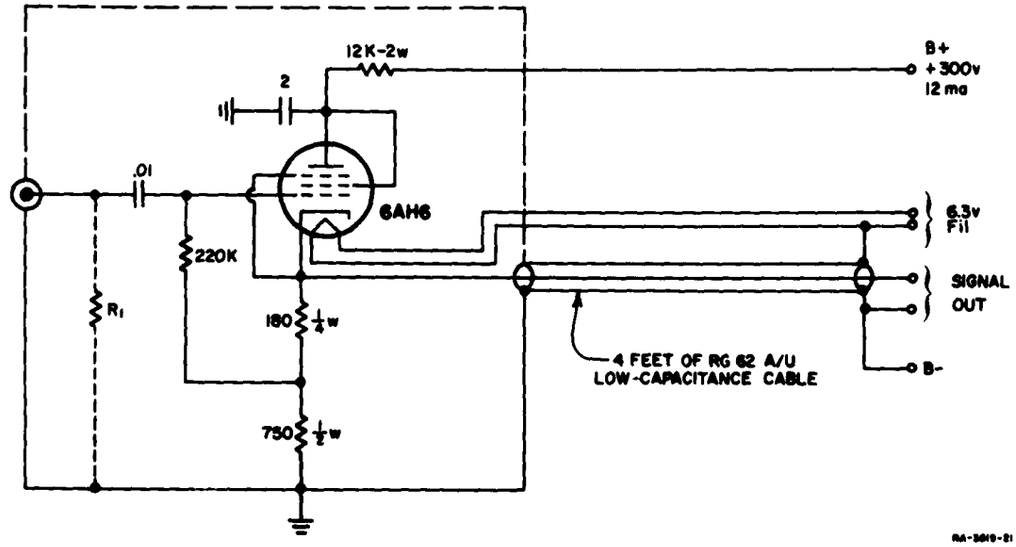

NOTE: R_1 = 6K FOR USE WITH VIDEO XTAL DETECTOR
R_1 OMITTED FOR USE WITH OSCILLOSCOPE VIDEO AMPLIFIER OUTPUT

FIG. 10 CATHODE-FOLLOWER CIRCUIT

The broadband video amplifiers consisted of the vertical amplifiers in Tektronix Model 514 oscilloscopes. These amplifiers have a 10-megohm input impedance and a video bandwidth that extends from about 20 cycles to 10 megacycles. Their output amplifier consists of a push-pull distributed-line amplifier driving the cathode ray tube, and in order to pick off an output signal without loading down this balanced-line amplifier, it is necessary to utilize a high-impedance, low-capacity, output device. A cathode-follower can perform this function admirably, so that the design shown in Fig. 10 was adapted to this purpose by removing the input resistor, R_1. With this output cathode follower attached, the over-all gain measured about 330. With an RF pulse power level of about

10 microwatts peak at the video crystal detector, an output pulse of 10 volts peak was obtained from the output cathode follower.

Output pulses from the Σ channel and the Δ channel are fed into the subtractor circuit, which is shown in detail in Fig. 11. This subtractor circuit is basically a simple dc bridge with the inputs applied to tubes V_3 and V_4, and the output taken from cathode follower V_5. Tubes V_1 and V_2 function as clamping diodes, the purpose of which is to restore the video waveform to the shape that it had at the video crystal detectors--i.e., after passing through one or more coupling capacitors, the waveform loses its "dc baseline" and becomes an ac signal with negative portions. The subtractor circuit will still subtract such ac signals, but its output

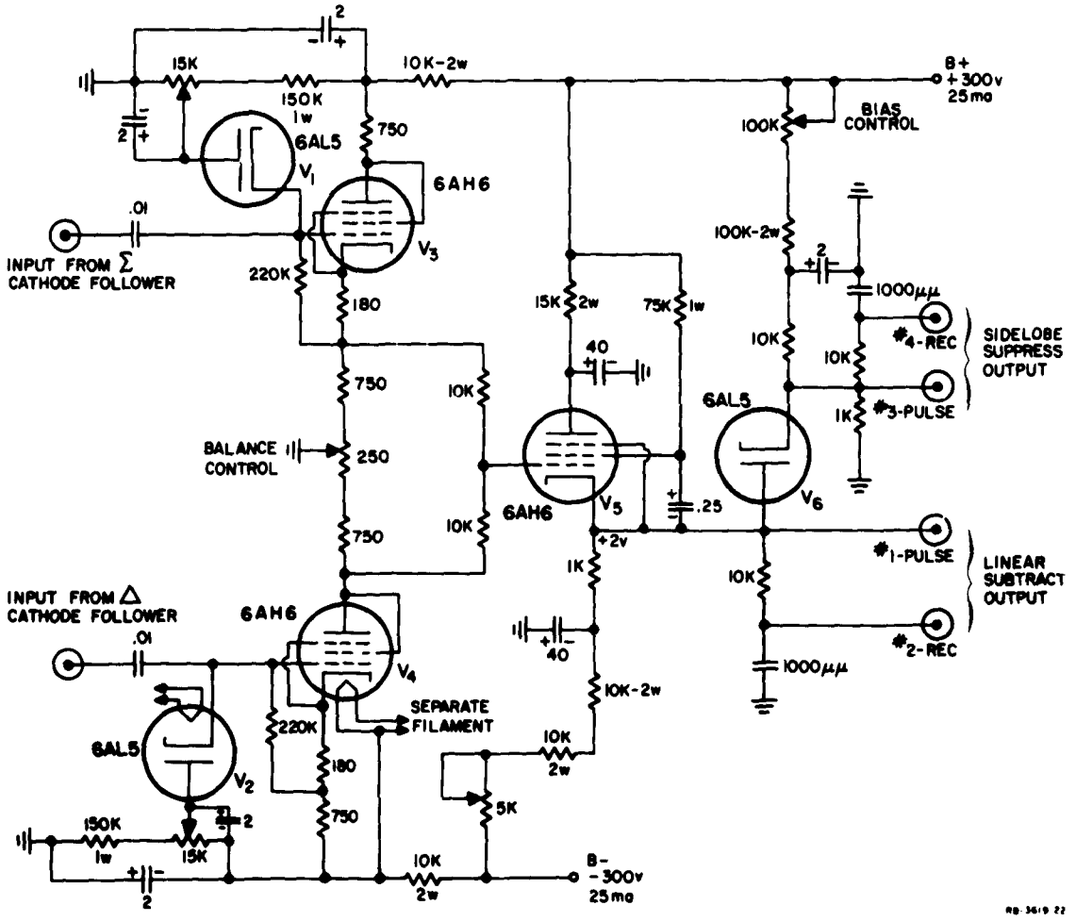

FIG. 11 SUBTRACTOR CIRCUIT

then no longer has a constant dc reference level for performing sidelobe suppression. Consequently, it is necessary to restore the waveform to its original dc baseline such that all portions of the signal are positive with respect to that baseline. This effect is of little significance when working with narrow pulse signals, where the dc baseline and the ac average level are very nearly the same, but it becomes very significant when working with wide pulses, square waves, or noise-like waveforms.

With an input pulse of 10 volts peak on either input, the subtractor circuit will give output pulses of about 2 volts peak, the output pulse being of positive sense if the input is on the Σ connector, and negative if the input is on the Δ connector. Ignoring the V_6 suppressor circuit for the moment, it will be noted that the output pulses are available for direct video presentation (for instance, on a monitor oscilloscope) at the linear subtract output connector labelled "#1-Pulse" in Fig. 11; or they are available for recording, after some filtering, at the linear subtract output connector labelled "#2-Rec." in Fig. 11. This simple subtractor circuit has too much dc drift to permit feeding a dc recorder directly from output connector No. 2--i.e., for pulse signals especially, the average dc voltage out of the subtractor is only about 10 or 20 millivolts at the most, and the dc drift in the circuit can sometimes equal this in a few minutes time. Therefore, it is necessary to remove the dc drift by means of a blocking condenser, and then recover the sense (positive or negative) of the ac output signal by means of synchronous detection.

A 1000-cycle synchronous detector[4] was available for use, but it required some amplification of the rather small rms signal (typically 10 millivolts maximum) obtained from pulse operation. Thus, a 1000-cycle tuned amplifier was inserted ahead of the synchronous detector. A Hewlett Packard 415B was used for this amplifier because it incorporates a decade attenuator and gain control that is convenient for adjusting gain to suit the large change in rms signal level that occurs when one switches back and forth between pulse and square-wave modulation. Since the amplifier is tuned to 1000 cycles, it has the further beneficial

effect of suppressing the noise that would otherwise come through from the broadband video circuits.

The reference signal for the synchronous detector is tapped off from the 1000-cycle sync signal that controls the transmitter modulation PRF (pulse repetition frequency) rate.

The output dc voltage from the synchronous detector, which has the same sense and is proportional to the subtractor circuit pulse output, is fed to a linear dc rectilinear recorder for automatically plotting the received power linearly as the antenna rotates.

Prior to taking patterns, the subtractor circuit was balanced and, also, the Σ channel gain and the Δ channel gain were balanced. The latter balance was achieved by disconnecting the interferometer portion of the antenna from the final magic tee so that this magic tee received energy only from the uniformly illuminated section of the antenna. Thus, the RF power was split equally into the Σ and Δ arms, and the appropriate variable attenuator was adjusted for a null (zero) in the subtractor circuit output.

A typical linear power pattern recorded on this antenna is shown in Fig. 12. A linear power scale, normalized to the recorded peak, and a calibrated angle scale have been added for convenience. In order to permit comparison with the theoretical pattern, Fig. 13 shows a plot of the theoretical pattern for this particular compound interferometer antenna, given as

$$|\Sigma|^2 - |\Delta|^2 \cong \frac{\sin \alpha}{\alpha} \qquad (5)$$

where

$\alpha = 8u = 8\pi(w/\lambda) \sin \theta$

$w = 32$ inches

$\lambda = 0.7874$ inch

θ = angle measured from the boresight direction .

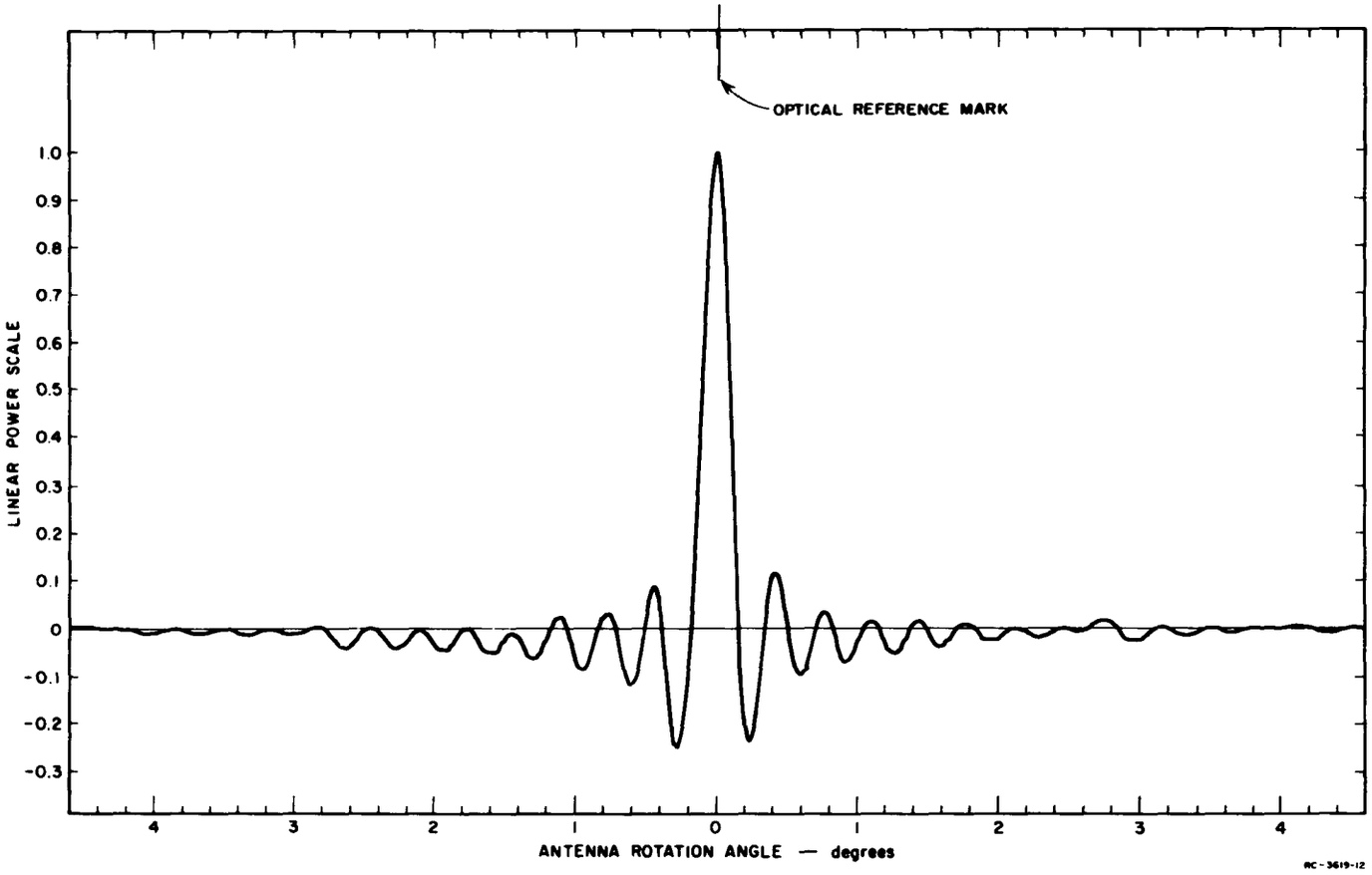

FIG. 12 E-PLANE LINEAR POWER PATTERN ON CROSS-CORRELATED COMPOUND INTERFEROMETER ANTENNA – FREQUENCY 15 GIGACYCLES

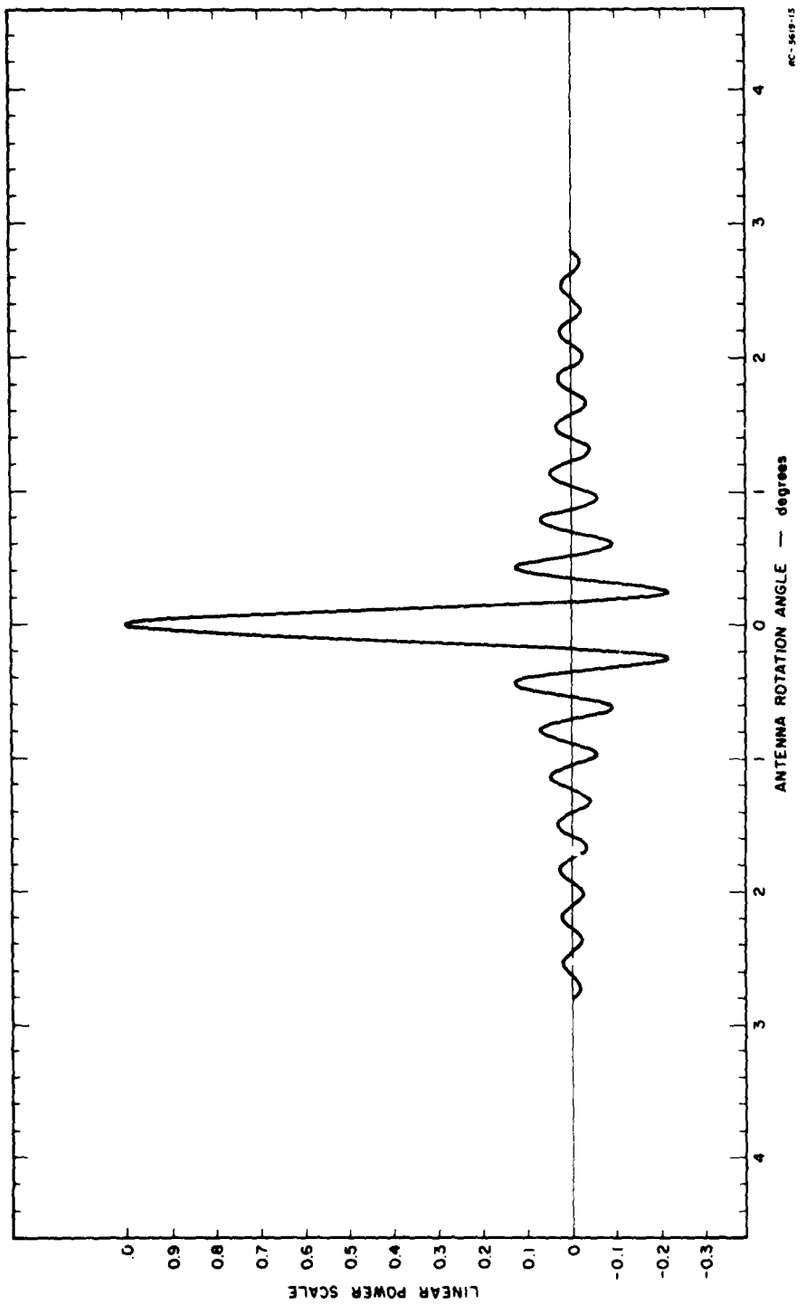

FIG. 13 SIN x/x LINEAR POWER PATTERN CALCULATED FOR THE EXPERIMENTAL COMPOUND INTERFEROMETER ANTENNA

The two patterns agree reasonably well, and it is believed that almost perfect agreement could be obtained if one had the time to make the necessary, corrective, experimental adjustments in the equipment. For instance, there is a tendency for the side-lobes to be more in the "negative-power" region than they should be.

Linear power patterns were taken with both pulse and square-wave modulation on the transmitting klystron, with essentially identical results. The pattern shown in Fig. 12 happens to have been taken using square-wave modulation.

It will be noted that the half-power beamwidth is about 0.2 degree, in very close agreement with the calculated beamwidth:

$$\theta_{\frac{1}{2}} = 34.4 \left(\frac{\lambda}{D}\right) = 0.205 \text{ degree} \qquad (6)$$

where D = 132 inches.

This is a good point at which to recall that the compound interferometer is a cross-correlation type of antenna--i.e., its power pattern is the Fourier transform of the cross-correlation of the uniformly illuminated section of aperture with the interferometer portion. The peculiar property of having negative-power sidelobes is a result of the cross-correlation processing in the receiver. The true patterns associated with the antenna are the sum power pattern, $|\Sigma|^2$ (see Fig. 8), and the difference power pattern, $|\Delta|^2$. The pattern of Fig. 12 is merely the result of subtracting these two, real, power patterns, so that a negative-power sidelobe is simply a negative receiver output voltage which is proportional to the difference between the two real power patterns.

D. Measurement of Sidelobe-Suppression Capabilities Utilizing a Non-Linear Element

The fact that the output power pattern of the compound interferometer results from receiver processing gives the antenna an advantage, with respect to conventional antennas, in that the pattern may be "shaped" or altered in many different ways simply through the use of further receiver

circuitry. For instance, against single sources (or targets), sidelobes can be suppressed to almost any degree desired by employing a suitable, biased, non-linear element. To demonstrate this capability experimentally, the simple biased diode circuit shown in Fig. 11 was tested.

When diode V_6 in Fig. 11 is biased above the voltage level of the cathode of V_5, all negative output pulses are suppressed from Outputs 3 and 4, and only positive pulses which exceed the bias voltage can pass through. Thus, by increasing the bias voltage until only the main-beam pulses are strong enough to come through, all sidelobes can be eliminated.

A very important characteristic of the compound interferometer with respect to this type of sidelobe suppression is that all sidelobes can be shifted downward into the negative region merely by increasing the gain of the Δ channel with respect to the Σ channel. For instance, if the gain of the Δ channel is increased to give a 3 db increase in the difference power pattern, $|\Delta|^2$, then the subtracted pattern,

$$(|\Sigma|^2 - 2\,|\Delta|^2) \qquad (7)$$

has almost no positive sidelobes.[1] The condition of all negative sidelobes is very desirable for two reasons: First, negative signals naturally require less bias voltage for achieving complete suppression by a non-linear element. Second, positive sidelobe signals are of the same sense as the main-beam signals, so that they can be eliminated only on the basis of amplitude difference, and this immediately limits the dynamic range of signal levels over which suppression can be achieved.

Sidelobe suppression is better demonstrated on a logarithmic power scale than it is on a linear power scale, so that the linear power recording arrangement shown in Fig. 9 was not used for recording suppression patterns. Instead, the suppressed 1000-cycle output from Connector No. 4 was passed through an attenuator-filter directly to the regular 40-db logarithmic antenna-pattern recorder. A series of four patterns was taken using different bias voltage settings, and these are reproduced in Fig. 14. These patterns graphically demonstrate the decrease in sidelobe level as the suppression bias voltage is increased.

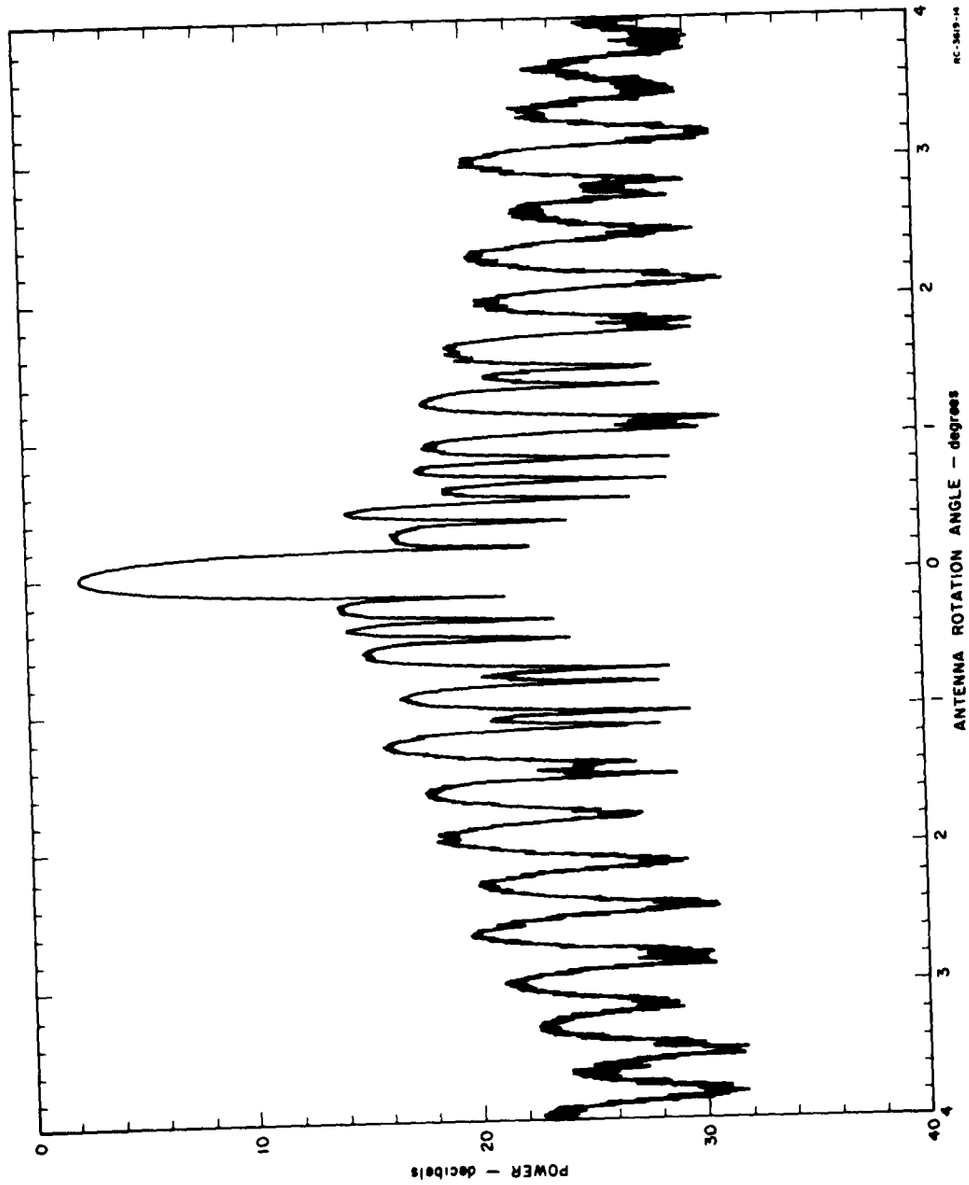

FIG. 14(a) SIDELOBE SUPPRESSION POWER PATTERNS ON COMPOUND INTERFEROMETER ANTENNA FOR 0 VOLTS BIAS – FREQUENCY 15 GIGACYCLES

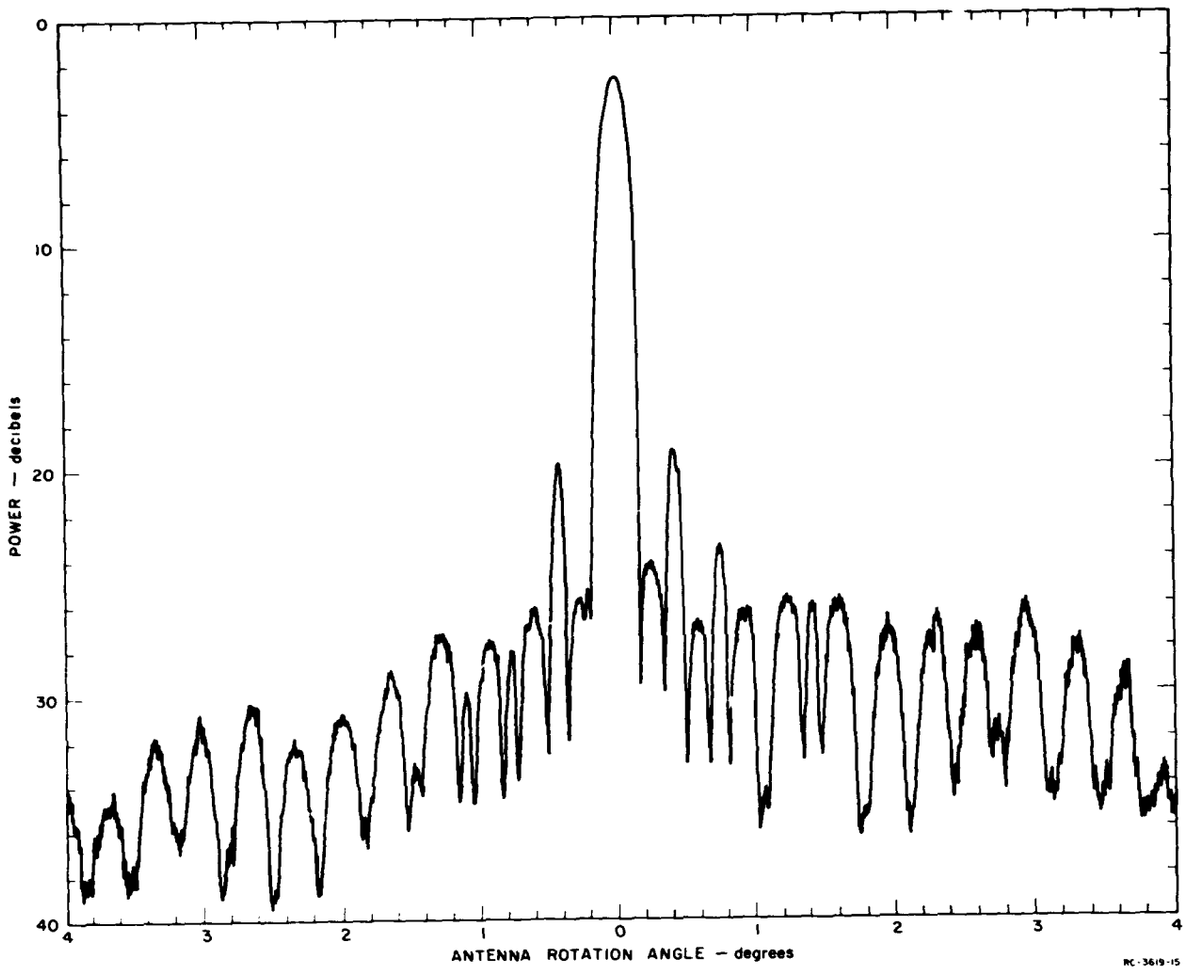

FIG. 14(b) SIDELOBE SUPPRESSION POWER PATTERNS ON COMPOUND INTERFEROMETER ANTENNA FOR 0.2 VOLTS BIAS – FREQUENCY 15 GIGACYCLES

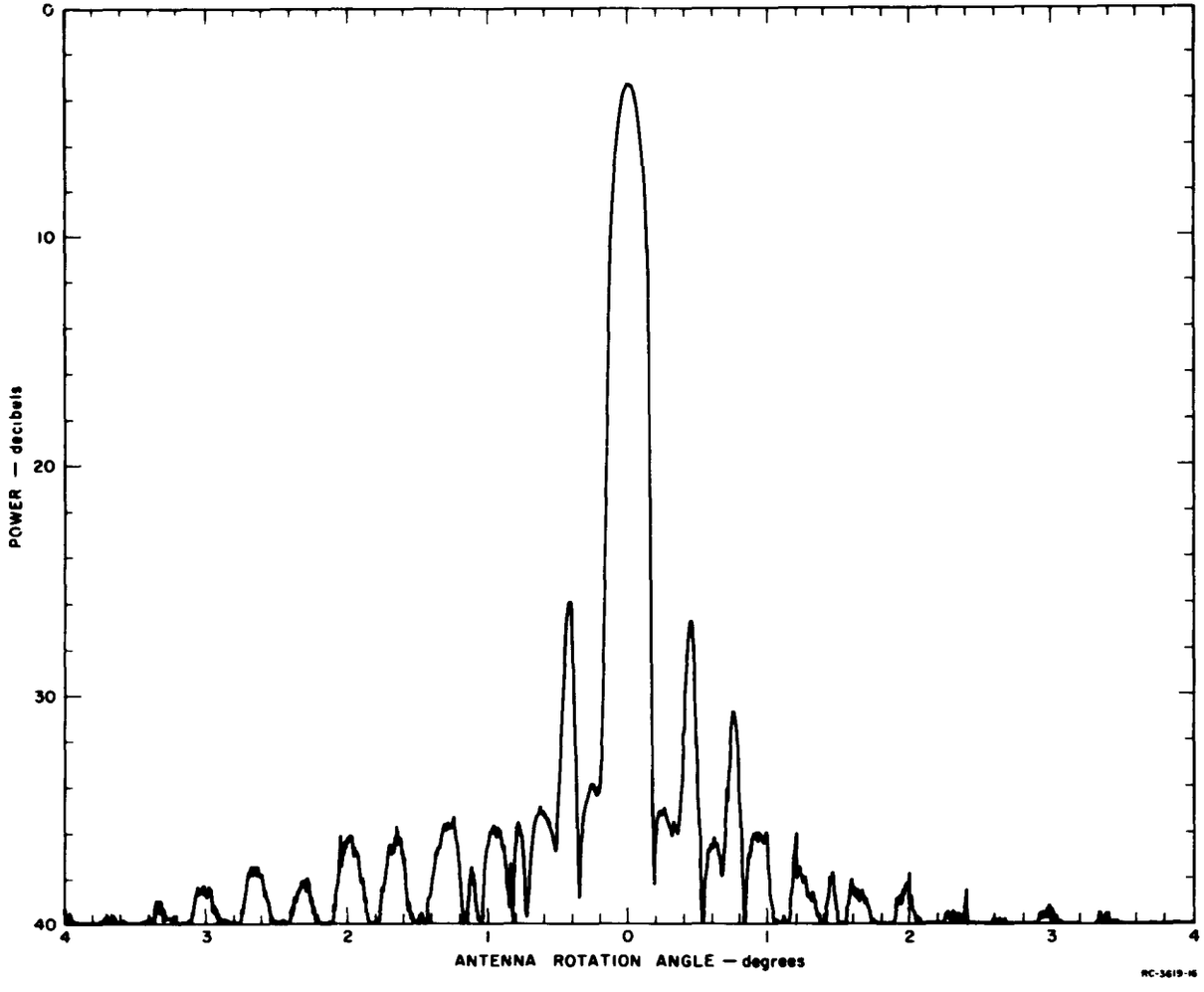

FIG. 14(c) SIDELOBE SUPPRESSION POWER PATTERNS ON COMPOUND INTERFEROMETER ANTENNA FOR 0.4 VOLTS BIAS – FREQUENCY 15 GIGACYCLES

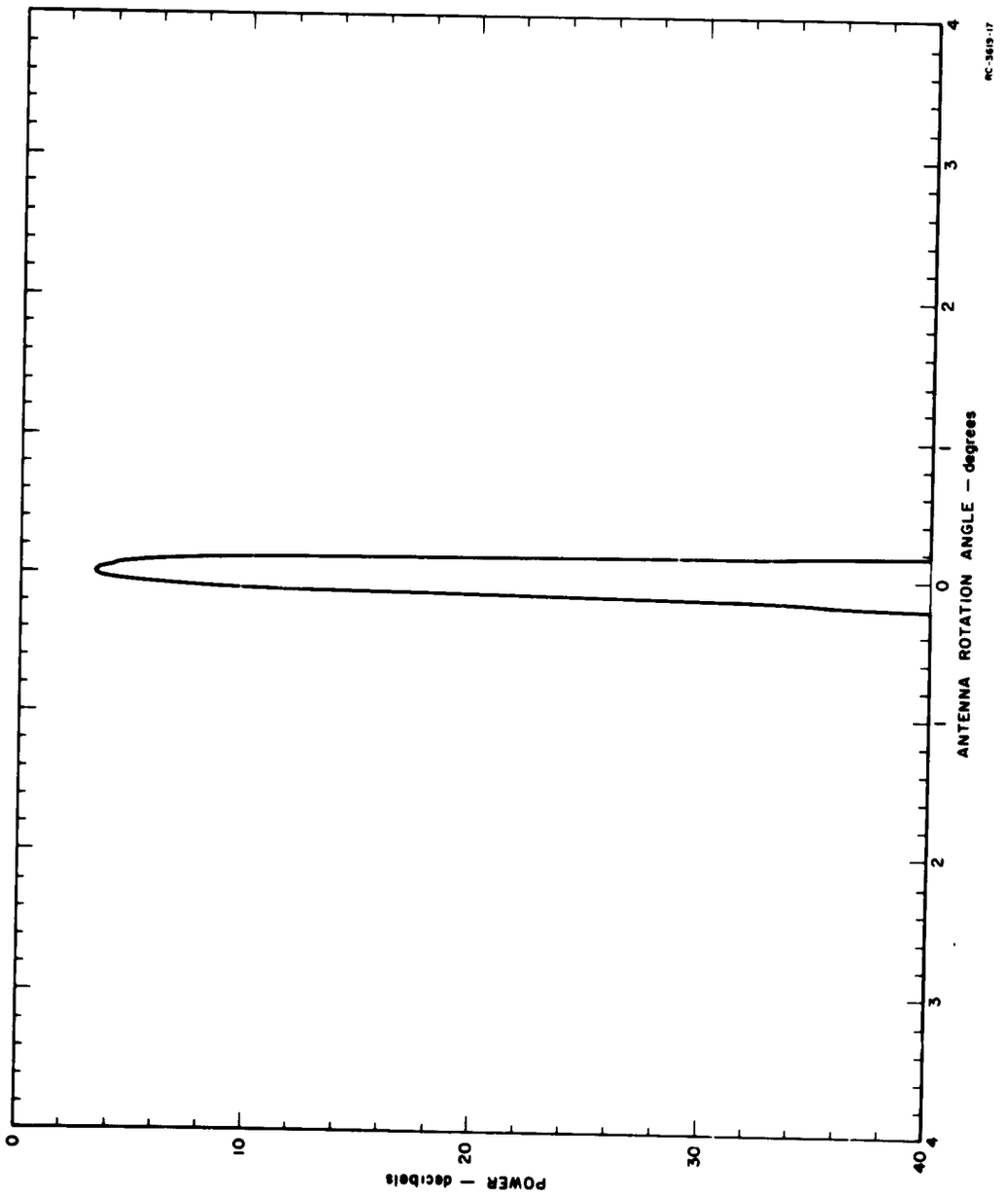

FIG. 14(d) SIDELOBE SUPPRESSION POWER PATTERNS ON COMPOUND INTERFEROMETER ANTENNA FOR 0.6 VOLTS BIAS – FREQUENCY 15 GIGACYCLES

Although the patterns in Fig. 14 are quite impressive, it must be noted that they demonstrate sidelobe suppression only under the ideal conditions of having a source (the transmitter) with a constant power level and a receiver with a constant gain. As the next step, it would be desirable and interesting to determine the dynamic range of source signal level (or, alternatively, receiver gain) over which effective sidelobe suppression could be maintained. For such a test, it would be necessary to equip the receiver with calibrated IAGC (instantaneous* automatic gain control), because a constant-gain receiver can never handle a dynamic range greater than that of its output circuitry, which in this case runs on the order of 10 db. The IAGC would have to control the Σ and Δ channel gains in parallel, of course, in order to keep their gain ratio constant. Unfortunately, incorporating IAGC into the present receiver would require the addition of two IF amplifiers plus the associated mixers and local oscillator, and the expense involved was considered to be too high for the limited project funds available. Thus, it was not possible to check out the dynamic range of source signal level over which effective sidelobe suppression could be maintained. It is assumed that this dynamic range value will be determined mainly by the level to which positive sidelobes can be reduced by increasing the ratio of the gain of the Δ channel with respect to the gain of the Σ channel. On the basis of previous calculations,[1] it appears reasonable to expect a range of from 15 to 30 db.

E. Sidelobe Suppression Obtained Through Use of Automatic Channel Signal Balancing

The previous subsection demonstrated the use of a non-linear element in obtaining sidelobe suppression. Another means for suppressing sidelobes on this antenna is to balance the sidelobe signals in the Σ and Δ channels through an AGC (automatic gain control) servo loop, whereupon the subtractor output will be reduced to near zero, even though the

---

* "Instantaneous" is used in a relative sense. It simply means that the gain control response must be fast with respect to the rate of change of received RF power as the antenna rotates.

sidelobe signals in the two channels may be of considerable magnitude. In order to demonstrate the channel balance method of sidelobe suppression, a simple electromechanical servo loop was assembled from available components and added to the receiver as shown in Fig. 15.

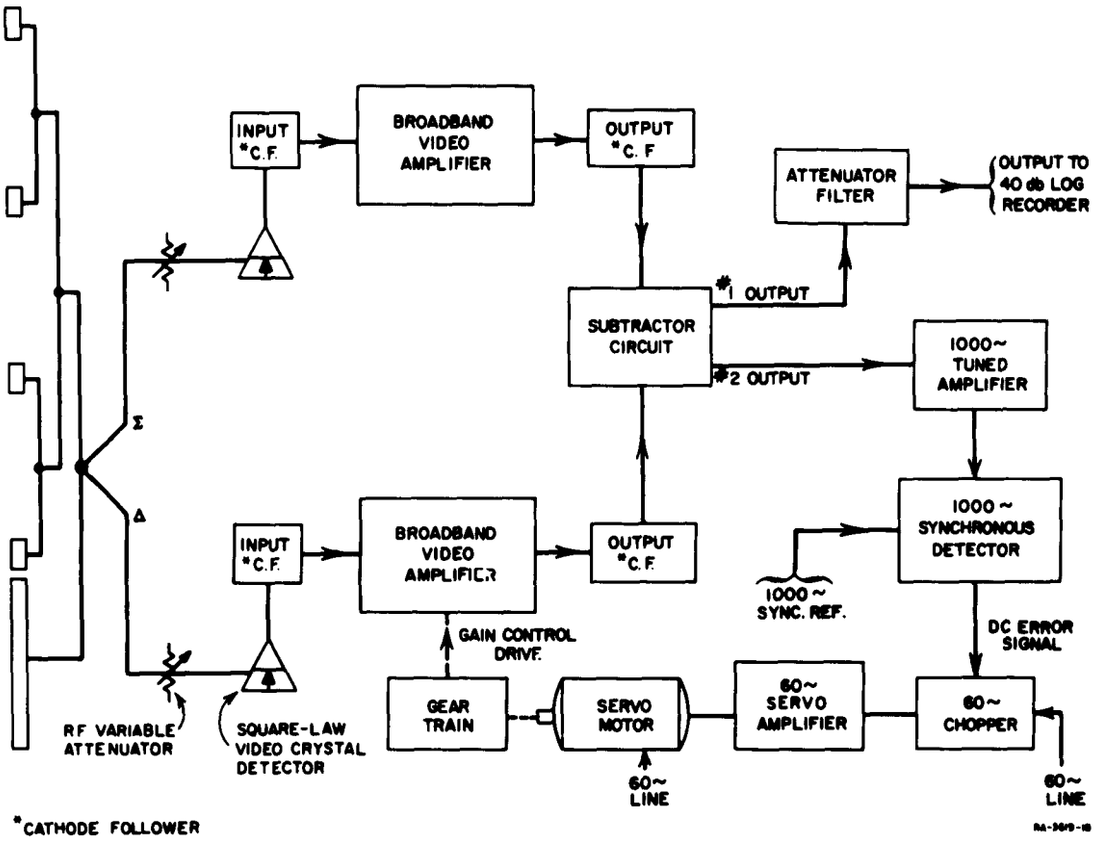

FIG. 15 BLOCK DIAGRAM OF RECEIVER WITH SIMPLE ELECTROMECHANICAL SERVO LOOP ADDED TO IT FOR CHANNEL SIGNAL BALANCING

The principle of operation is that the servo will always try to keep the subtractor output at zero--i.e., if the subtractor output is a positive signal, the servo will drive to increase the gain of the Δ channel, thereby increasing the magnitude of the Δ channel signal and reducing the positive output. Theoretically, sidelobe signals always exist in both channels simultaneously, and will therefore be eliminated from the subtractor output by the servo balancing action, whereas

main-beam signals (at the peak) exist only in the Σ channel and are not affected by the servo action. Thus, the servo should permit only the peak of the main beam to appear at the output of the subtractor circuit.

From a practical servo standpoint, the gain-control problem is not too severe, since (as mentioned earlier) the power pattern obtained from doubling the gain of the Δ video amplifier,

$$(|\Sigma|^2 - 2\,|\Delta|^2) \tag{7}$$

has almost no positive sidelobes. Thus, if the difference amplifier is set up initially to have twice the gain of the sum amplifier at maximum position, then the servo can always achieve balance in the sidelobe region merely by driving the gain control of the difference amplifier alone. A gain-control range of about 10 to 1 should be sufficient.

Unfortunately for the experimental test, the gain-control range of the Δ video amplifier (a Tektronics 514 Oscilloscope) was only about 3 to 1, so that although normally positive sidelobes could be suppressed, the normally negative sidelobes could only be partially suppressed--i.e., the servo could not reduce the gain of the Δ video amplifier far enough to cancel the normally negative sidelobes. Despite this deficiency in gain-control range, a test pattern was run to see what results the servo would give on positive sidelobes and also on the main beam (which is also positive). The results are shown in Fig. 16 where, for convenience, the various lobes are labelled positive or negative by means of $\pm$ signs. Comparing Fig. 16(b), in which the servo was on, with Fig. 16(a), in which the servo was off, one will note the following:

(1) Negative sidelobes were reduced only by 2 or 3 db, as expected, because of the lack of sufficient gain-control range in this particular servo system.

(2) Positive sidelobes were reduced by about 10 to 15 db, such that their average level is better than 20 db below the peak of the main beam.

(3) The main beam itself was sharpened by a factor of about 25 percent.

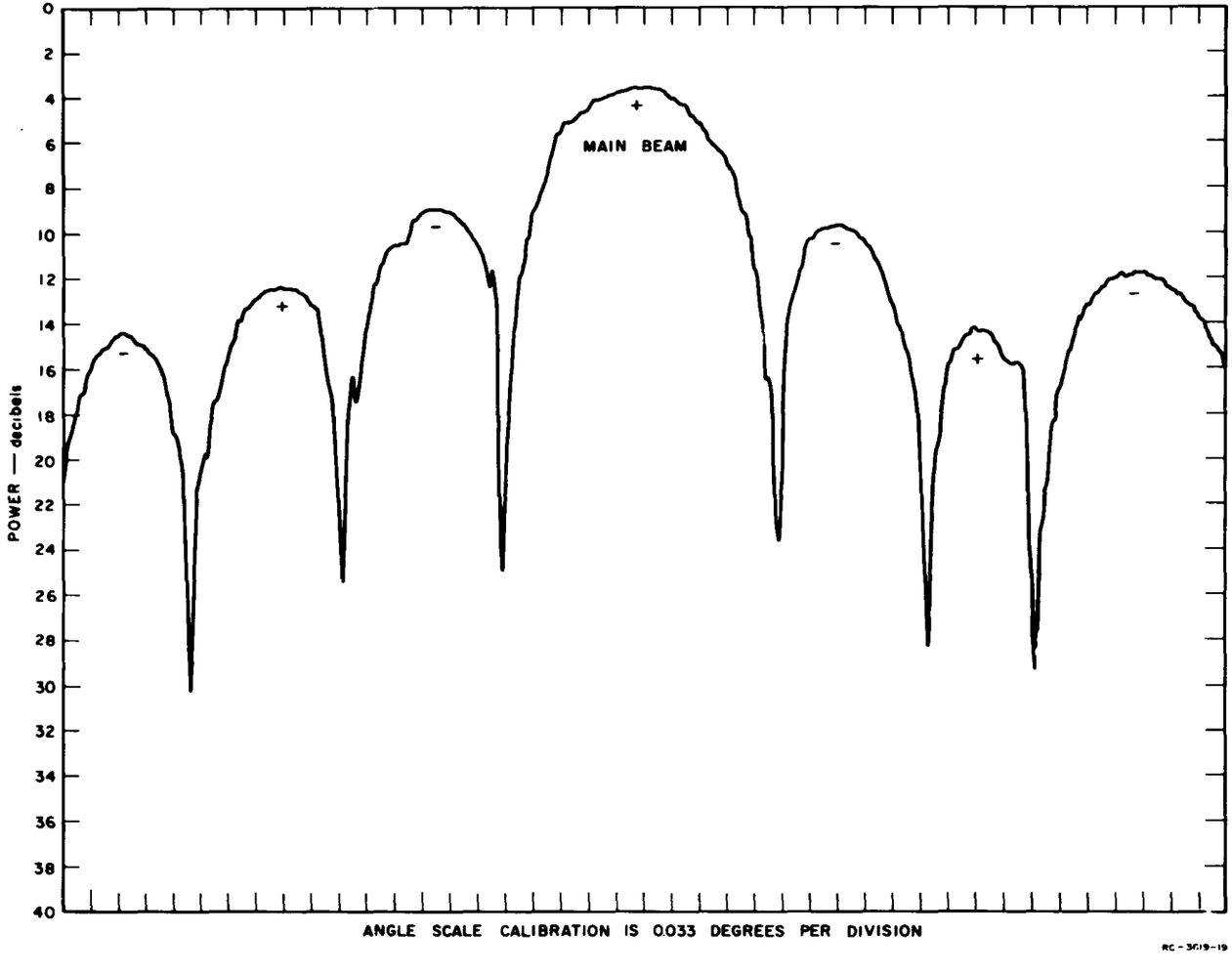

FIG. 16(a) SIDELOBE-SUPPRESSION POWER PATTERNS OBTAINED BY UTILIZING A CHANNEL SIGNAL BALANCING SERVO LOOP – SERVO OFF

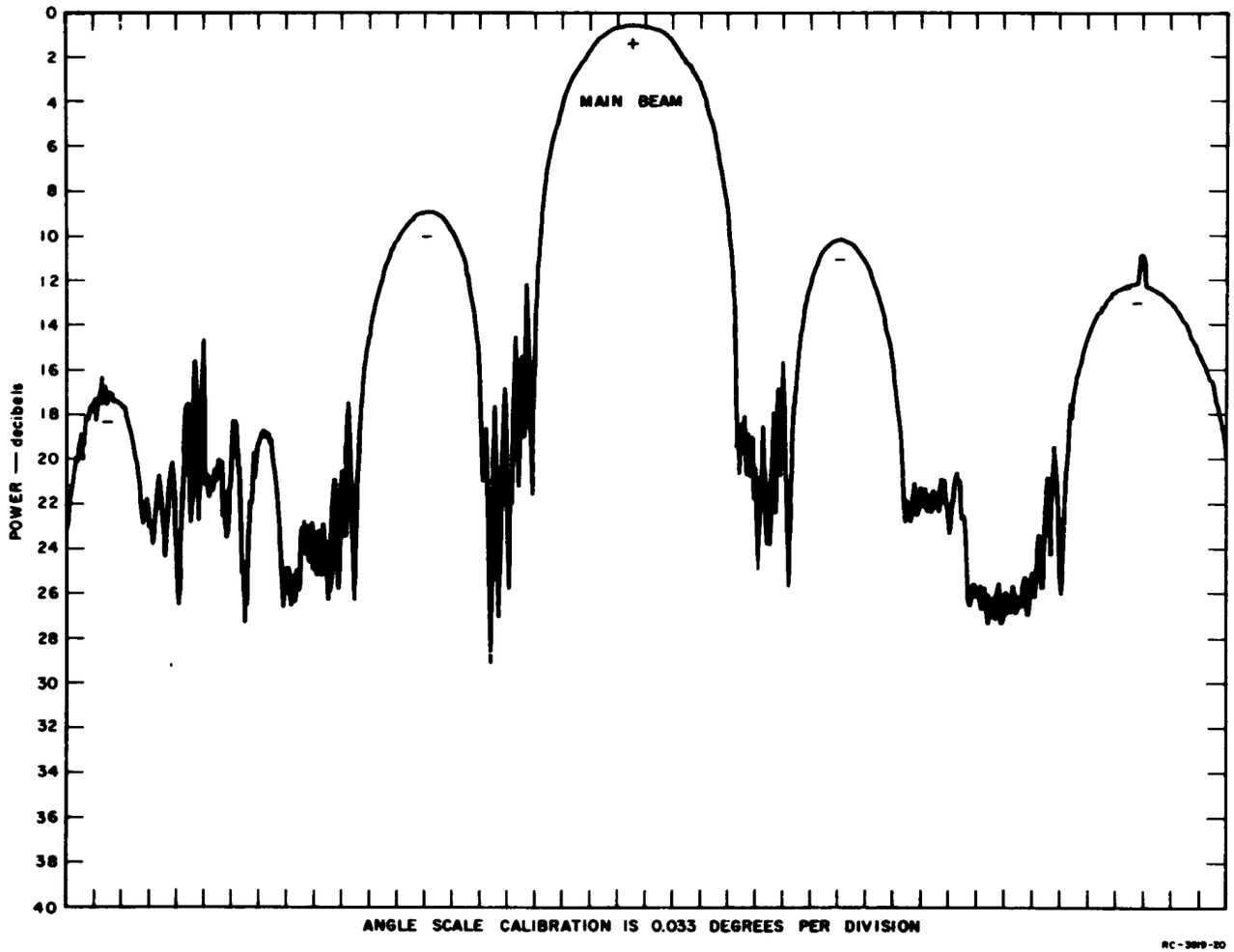

FIG. 16(b) SIDELOBE-SUPPRESSION POWER PATTERNS OBTAINED BY UTILIZING A CHANNEL SIGNAL BALANCING SERVO LOOP – SERVO ON

Thus, despite the deficiencies in the particular equipment employed in this test, the principle of sidelobe suppression through use of a channel-balancing, AGC servo loop was definitely demonstrated. There is no question but what the negative sidelobes could have been suppressed as much as the positive sidelobes were suppressed, if the video amplifier had had sufficient gain-control range.*

In a radar-type receiver, channel-balancing could be performed in a far superior manner by controlling the gain of the Δ channel IF amplifier. Being ahead of the square-law detector, the gain-control range needed at the IF amplifier would only be about 3 to 1, compared to the 10-to-1 range needed at the video amplifier in the present test set-up. In a practical radar system, one would also have to have a far faster response time in the AGC servo loop, since response time must be fast with respect to beam-position dwell time.

As a sidelobe-suppression technique, channel-signal balancing is more desirable than the use of a non-linear element, because in the non-linear element technique, a negative bias is produced at the subtractor circuit output which is proportional to the level of the negative sidelobe that is eliminated, so that in multiple-source situations, a desired weak source might be "blanked out" by the sidelobe bias produced by a nearby strong source. In the signal-balancing technique there is no such bias to overcome, so that a weak source cannot be blanked out by a strong source, at least not within the dynamic range limits of operation of the AGC loop. In this respect, the suppressed sidelobes achieved by signal balancing behave in a manner similar to the true sidelobes associated with a conventional antenna. A limitation on this technique is that sidelobes cannot be suppressed below the level determined by the balance error signal of the AGC servo loop, so that sidelobe suppression of more than

---

* The gain-control range situation could have been remedied, of course, either by alteration of the oscilloscope video amplifier or by having the servo drive the RF attenuator in the Δ channel, but a limited time schedule on the part of the author prevented making these alterations.

about 20 db would be difficult to achieve, considering the usual dynamic range limitations of receiver circuitry. Another factor to consider, from the standpoint of a practical radar system, is that channel-signal balancing is applicable mainly to RF modulation waveforms that result in a high average power level, such as square-wave modulation or noise modulation. The reason for this may be found in the gain-bandwidth requirements of the servo loop. The fast servo response time required in most radar applications[2] demands a wide enough bandwidth that the amount of gain that can be tolerated in the servo loop becomes limited, thereby setting the minimum average voltage level of the error signal which, in turn, sets the minimum average RF power level for which the servo will operate well.

As a matter of interest, Fig. 17 shows patterns taken on two transmitting sources which were spaced 13 feet apart at the pattern range distance of 1320 feet. Source A was square-wave modulated whereas Source B was pulse modulated with a pulse width of 10 microseconds. The repetition rate was 1000 cps. The two sources gave approximately equal peak power at the receiver, so that the average power level of Source B was about 17 db below the average power level of Source A. The pattern in Fig. 17(a) was taken without sidelobe suppression, and it will be noted that it is impossible to distinguish Source B from the sidelobes of Source A. The pattern in Fig. 17(b) was taken with sidelobe suppression, whereupon Source B is easily recognized. The pattern spacing between the two sources is 17 divisions or 34 minutes (2 minutes or 0.033 degree per division), which is exactly the angle that is subtended by the 13-foot spacing at 1320-foot range. Both channel-signal balancing and non-linear diode suppression were utilized in obtaining the pattern shown in Fig. 17(b). Because of the difference in average power level, the channel-signal-balancing servo worked well on the sidelobes of Source A, but would not work well on the sidelobes of Source B. The non-linear diode suppressor, on the other hand, worked well on the sidelobes of either source, and was necessary for this particular test in order to remove the negative sidelobes from Source A that were left by the channel-signal-balancing servo.

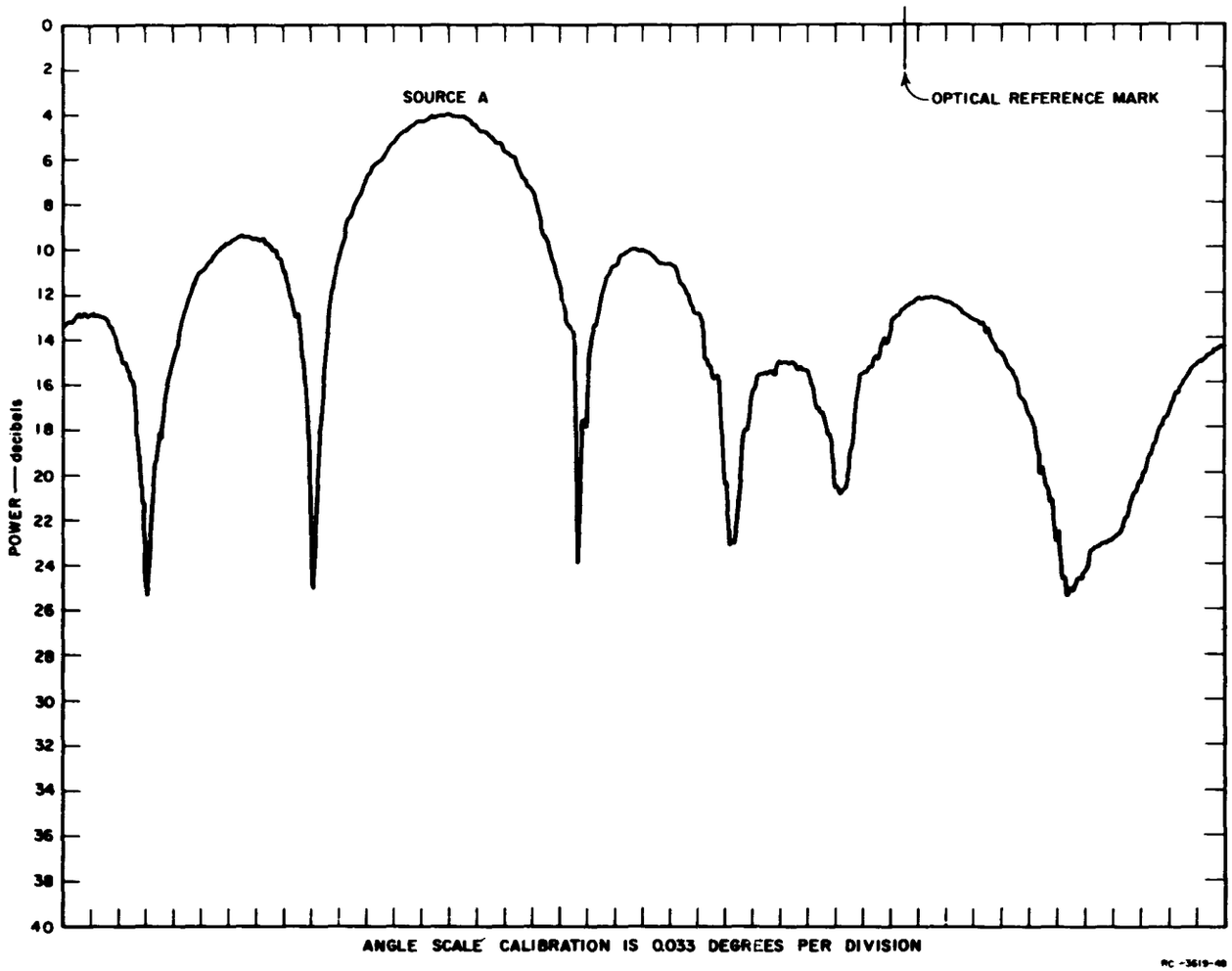

FIG. 17(a) PATTERNS TAKEN ON TWO SIMULTANEOUSLY TRANSMITTING SOURCES SPACED 13 FEET APART AT A DISTANCE OF 1320 FEET. SOURCE A SQUARE-WAVE MODULATED; SOURCE B PULSE-MODULATED AND ABOUT 17 db BELOW SOURCE A IN AVERAGE POWER LEVEL. WITHOUT SIDELOBE SUPPRESSION.

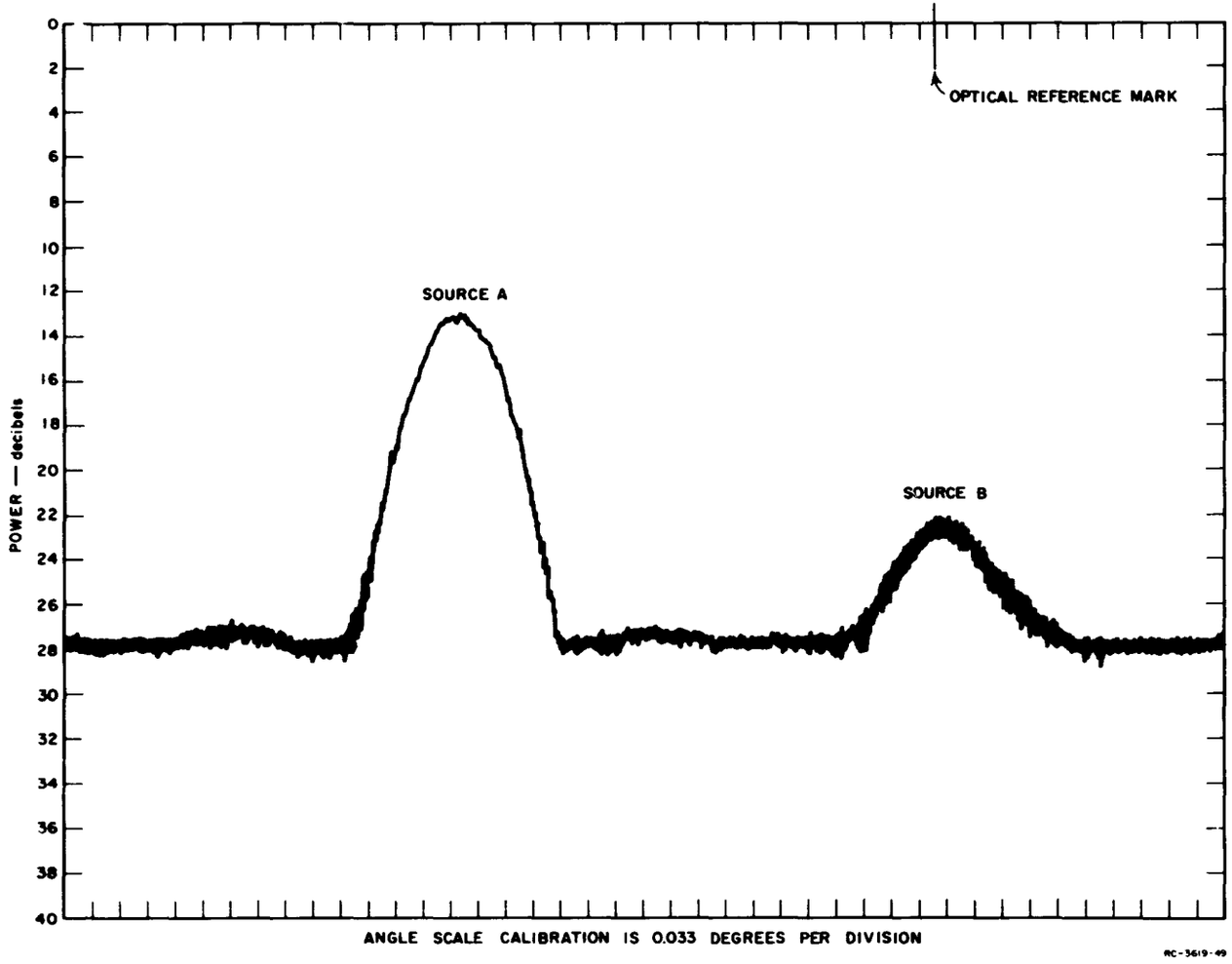

FIG. 17(b) PATTERNS TAKEN ON TWO SIMULTANEOUSLY TRANSMITTING SOURCES SPACED 13 FEET APART AT A DISTANCE OF 1320 FEET. SOURCE A SQUARE-WAVE MODULATED; SOURCE B PULSE-MODULATED AND ABOUT 17 db BELOW SOURCE A IN AVERAGE POWER LEVEL. WITH SIDELOBE SUPPRESSION.

This test showed that the two sidelobe-suppression techniques are complementary, and that it is advantageous to use them simultaneously. It would be particularly interesting to test their combined sidelobe-suppression capability in a multiple-source environment, using a receiver equipped with calibrated IAGC. The object of the test, of course, would be to determine the dynamic range of signal level over which it is possible to detect a weak source in the presence of one or more strong sources, since this is a primary requirement for successful radar operation.

III CONCLUSIONS

An experimental compound interferometer antenna has been constructed and tested in order to help evaluate its applicability as a possible radar antenna.

On the whole, its measured patterns conformed quite closely to the patterns arrived at in the theoretical analysis. Alignment adjustments in the antenna-waveguide feed network were somewhat critical, but were considered to be in keeping with the narrow beamwidth of the antenna, which measured about 12 minutes.

The flexibility and ease of receiver control over the output power pattern of this antenna proved to be a most interesting feature, and contrasted sharply with the difficulty of pattern control experienced with conventional antennas. For instance, preparations for recording the familiar sin α/α linear power pattern associated with this antenna consisted only of making a few balance adjustments in the receiver.

Two different sidelobe-suppression techniques were tested; one utilizing a non-linear element at the subtractor circuit output, and one using an automatic channel-signal-balancing servo. The former technique has the advantage of operating equally well on any type of envelope modulation waveform and permitting a more complete suppression, but it has the disadvantage of developing a "sidelobe bias" which could be harmful in multiple-source situations. The latter technique has the advantage of not having any "sidelobe bias" effect, but its suppression capability is limited to perhaps 20 db, and it is applicable mainly to modulation waveforms that result in a high average power level--i.e., a large duty factor. An advantage of both techniques is a marked sharpening of the main beam. Also, it was found to be very advantageous to combine the two techniques and use them simultaneously.

On the basis of the sidelobe-suppression performance obtained from this experimental model, it is concluded that the compound interferometer antenna could be applied to radar use in those situations where its

advantages of high resolution and aperture conservation outweigh its disadvantage of requiring the implementation of sidelobe suppression, which results in a more complicated receiver. It should be noted that the compound interferometer is naturally suited to sidelobe-suppression techniques and does not require an auxiliary antenna for this purpose.

Although this experimental model had a large aperture in terms of wavelengths and was operated at a high microwave frequency, there is no fundamental reason for not building a compound interferometer with a much smaller aperture in terms of wavelengths and operating at a low frequency. In fact, the aperture conservation and high resolution permitted by the compound interferometer is probably of greater economic importance at HF and UHF frequencies than it is at microwave frequencies, because of the high cost per element and the real estate required at the lower frequencies.

ACKNOWLEDGMENT

The author wishes to acknowledge the assistance of A. L. Pierce, Engineering Assistant, in assembling and testing the compound interferometer under an inconvenient time schedule.

REFERENCES

1. W. F. Gabriel and M. G. Andreasen, "Investigations of Methods of Scanning The Beams of Large Antennas," Scientific Report 12, SRI Project 2184, Contract AF 19(604)-2240, Stanford Research Institute, Menlo Park, California (September 1960).

2. W. F. Gabriel, "Investigations of Methods of Scanning The Beams of Large Antennas," Part II of Final Report, Contract AF 19(604)-2240, SRI Project 2184, Stanford Research Institute, Menlo Park, California (March 1961), CONFIDENTIAL.

3. R. W. Friis and A. S. May, "A New Broadband Microwave Antenna System," Communications and Electronics, No. 35, pp 97-100 (March 1958).

4. D. Middleton and R. M. Hatch, Jr., "The Coherent Detector," Tech. Report 80, ONR Contract N5 ori-76, Cruft Lab., Harvard University, Cambridge, Mass. (7 July 1949).

STANFORD RESEARCH INSTITUTE | MENLO PARK, CALIFORNIA

Regional Offices and Laboratories

SOUTHERN CALIFORNIA LABORATORIES
820 Mission Street
South Pasadena, California

WASHINGTON OFFICE
808 17th Street, N.W.
Washington 5, D.C.

NEW YORK OFFICE
270 Park Avenue, Room 1770
New York 17, New York

DETROIT OFFICE
The Stevens Building
1025 East Maple Road
Birmingham, Michigan

EUROPEAN OFFICE
Pelikanstrasse 37
Zurich 1, Switzerland

Representatives

HONOLULU, HAWAII
Finance Factors Building
195 South King Street
Honolulu, Hawaii

LONDON, ONTARIO, CANADA
85 Wychwood Park
London, Ontario, Canada

LONDON, ENGLAND
15 Abbotsbury Close
London W. 14, England

MILAN, ITALY
Via Macedonio Melloni 40
Milano, Italy